Electronic Supplementary Material (ESI) for Nanoscale Advances.


# The Role of Nanoparticle Size and Ligand Coverage in Size Focusing of Colloidal Metal Nanoparticles

Saeed Mozaffari,[a] Wenhui Li,[a] Mudit Dixit,[b] Soenke Seifert,[c] Byeongdu Lee,[d] Libor Kovarik,[e] Giannis Mpourmpakis,[b] and Ayman M. Karim[a,*]

[a] Virginia Polytechnic Institute and State University, Blacksburg, VA 24060, United States

[b] Department of Chemical Engineering, University of Pittsburgh, Pittsburgh, Pennsylvania 15261, United States

[c] Advanced Photon Source, Argonne National Laboratory, Argonne, IL 60439, United States

[d] X-ray Science Division, Argonne National Laboratory, Argonne, IL 60439, United States

[e] Environmental Molecular Science Laboratory, Pacific Northwest National Laboratory, Richland, Washington, 99352, United States

* Corresponding author, amkarim@vt.edu

## Nomenclature

| | |
|---|---|
| $a_t$ | Total surface area of a nanoparticle |
| $a_{TOP}$ | Surface area covered by one TOP ligand |
| $a_l$ | Capped surface area of a nanoparticle |
| $A$ | Kinetically active precursor |
| $AL$ | Ligand-precursor complex |
| $B$ | Ligand-free surface atom |
| $BL$ | Ligand-capped surface atom |
| $D$ | Particle diameter |
| $D_{ave}$ | Average particle size |
| $E_0$ | Intrinsic activation energy |
| $E_a$ | Activation energy |
| $E_{a\text{-}G}$ | Activation energy for surface growth |
| $E_{a\text{-}G0}$ | Activation energy for surface growth at zero coverage |
| $E_{a\text{-}L}$ | Activation energy for ligand-nanoparticle binding |
| $E_{a\text{-}L0}$ | Activation energy for ligand-nanoparticle binding at zero coverage |
| $F_c$ | Average fractional surface coverage |
| $G$ | Growth rate of nanoparticle |
| $J$ | Sum of normalized squared errors |
| $k_{1\text{-nuc}}$ | Reduction-nucleation rate constant |
| $k_{2\text{-growth}}$ | Growth rate constant |
| $k_{3\text{-f}}$ | Forward reaction rate constant for the precursor-ligand association step |
| $k_{3\text{-r}}$ | Reverse reaction rate constant for the precursor-ligand association step |
| $k_{4\text{-f}}$ | Forward reaction rate constant for the particle-ligand association step |
| $k_{4\text{-r}}$ | Reverse reaction rate constant for the particle-ligand association step |
| $K$ | Rate of nanoparticle surface coverage |
| $K_{eq}$ | Equilibrium constant |
| $L$ | Free ligand |
| $M_{0,0}$ | Total number of particles per reaction volume |
| $M_{1/3,0}$ | Relates to sum of diameter of all nanoparticles per reaction volume |
| $M_{2/3,0}$ | Relates to total surface area of all nanoparticles per reaction volume |
| $M_{1,0}$ | Total volume of all nanoparticles per reaction volume |
| $M_{0,1}$ | Total ligand covered surface area of all nanoparticles per reaction volume |
| $M_{i,k}$ | Moment of size distribution |
| $M_w$ | Molecular weight |
| $n_c$ | Number of atoms per nucleus |
| $n$ | Number density |
| $N_A$ | Avogadro's number |
| $N_p$ | Concentration of particles |

| | |
|---|---|
| $N_{sites}$ | Number of surface sites per unit area |
| $\dot{N}$ | Nucleation rate |
| $P$ | Polydispersity |
| $r$ | Particle radius |
| $R$ | Ideal gas constant |
| $t$ | Time |
| T | Temperature |
| $v_{pd}$ | Volume of a Pd atom |
| $V_c$ | Volume of a nucleus |
| $\alpha$ | Transfer coefficient |
| $\alpha_G$ | Transfer coefficient for nanoparticle surface growth |
| $\alpha_L$ | Transfer coefficient for ligand-nanoparticle binding |
| $\theta$ | Surface coverage |
| $\rho$ | Density |
| $\sigma$ | Standard deviation (width of distribution) |
| $\Delta H$ | Enthalpy of reaction |
| $\Delta H_{0-L}$ | Enthalpy of reaction for ligand-nanoparticle binding at zero coverage |
| $\Delta H_{0-G}$ | Enthalpy of reaction for nanoparticle surface growth at zero coverage |
| $\Delta H_L$ | Enthalpy of reaction for ligand-nanoparticle binding |
| $\Delta H_G$ | Enthalpy of reaction for nanoparticle surface growth |

**Estimation of Concentration of Nanoparticles ($N_p$) from In-Situ SAXS Measurements.** We can obtain nanoparticles size, concentration of nanoparticles, polydispersity, and the absolute intensity *I(q=0)* based on the SAXS fitting analysis. We used pure water (as a standard) for calibration of intensity to the absolute scale[1]. For polydisperse spherical shape nanoparticles, the scattering intensity *I(q)* is defined as[2]

$$I(q) = N_p \int_0^\infty f(r)\, {V_p}^2 P(q) dr \qquad (1A)$$

where $N_p$ is the concentration of nanoparticles, $V_p$ the volume of nanoparticle, *P(q)* the single particle form factor. *f(r)* is the Schultz distribution factor[3] and can be written as follows[3]:

$$f(r) = \frac{r^z}{\Gamma(z+1)} \left[\frac{z+1}{r_{ave}}\right]^{z+1} \exp\left(-\frac{r(z+1)}{r_{ave}}\right) \qquad (2A)$$

where $(r_{avg}/\sigma)^2 = z + 1$.

Here, $r_{ave}$ is the average nanoparticle radius, $z$ relates to the width of distribution, and $\Gamma$ is the gamma function.

The scattering intensity (once $q \longrightarrow 0$) can be written as[2, 4]

$$I(q = 0) = N_p \langle {V_p}^2 \rangle (\Delta\rho)^2 \qquad (3A)$$

where $\langle {V_p}^2 \rangle$ and $\Delta\rho$ are the average square of nanoparticle volume and the scattering length density difference between metal nanoparticle and solvent, respectively. *I(q=0)* is obtained via extrapolation as it

cannot be obtained from the experiment. Based on eq. 3A, the concentration of nanoparticles can be determined as follows[2, 4]:

$$N_p = \frac{I(q=0)}{(\Delta\rho)^2\langle {V_p}^2\rangle} \qquad (4A)$$

**Damköhler Number (*Da*).** The ratio of reaction rate to diffusion rate (i.e. *Da*) can be calculated as $Da \approx r^2(\frac{k_{3-growth}[A]}{D_{ab}})$[5].[$A$] is the metal concentration, $k_{3-growth}$ is the rate constant for surface growth, and *r* is the radius of the growing nanoparticle. $D_{ab}$ is the diffusion coefficient of metal complex in pyridine or toluene and it can be estimated based on Stokes-Einstein equation[6]; $D_{ab} = \frac{k_B T}{6\pi R_e \mu}$. Here $T, k_B, R_e$ and μ represent the absolute temperature, the Boltzmann constant, the effective radius of the diffusing species (for our system, metal complex which is bound with ligand), and the solvent viscosity, respectively. The value of *Da* for the nanoparticles with the size of 2 nm was estimated to be in the range of $10^{-8}$-$10^{-9}$. This further confirms that the growth is reaction-limited.

## Differential Equations for Moments of Size Distribution and Reactants Concentration:

**Moments of Size Distribution**

$$\frac{dM_{0,0}}{dt} = \frac{k_{2-nuc}[A]N_A}{n_c} = \dot{N}$$ Nucleation rate per reaction volume

$$\frac{dM_{1/3,0}}{dt} = \dot{N}v_c^{1/3} + \frac{1}{3}(36\pi)^{1/3} v_{pd} N_{sites} k_{3-growth}[A](1-F_c)M_{0,0}$$ Size change rate of all nanoparticles per reaction volume

$$\frac{dM_{2/3,0}}{dt} = \dot{N}v_c^{2/3} + \frac{2}{3}(36\pi)^{1/3} v_{pd} N_{sites} k_{3-growth}[A](1-F_c)M_{1/3,0}$$ Area change rate of all nanoparticles per reaction volume

$$\frac{dM_{1,0}}{dt} = \dot{N}v_c + v_{pd} N_{sites} k_{3-growth}[A][(36\pi)^{1/3} M_{2/3,0} - M_{0,1}]$$ Volume change rate of all nanoparticles per reaction volume

$$\frac{dM_{0,1}}{dt} = a_{TOP} N_{sites} k_{4-f}[L][(36\pi)^{1/3} M_{2/3,0} - M_{0,1}] - a_{TOP} N_{sites} k_{4-r} M_{0,1}$$ Surface coverage change rate of all nanoparticles per reaction volume

$$F_c = \frac{M_{0,1}}{(36\pi)^{1/3} M_{2/3,0}}$$ Average fractional surface coverage

$M_{i,k} = 0$ at time=0

**Reactants Concentration**

$$\frac{d[A]}{dt} = -\frac{n_c}{N_A}\dot{N} - \frac{N_{sites}}{N_A} k_{3-growth}[A][(36\pi)^{1/3} M_{2/3,0} - M_{0,1}] - k_{1-f}[A][L] + k_{1-r}[AL]$$

$$\frac{d[AL]}{dt} = k_{1-f}[A][L] - k_{1-r}[AL]$$

$$\frac{d[B+BL]}{dt} = \frac{n_c}{N_A}\dot{N} + \frac{N_{sites}}{N_A} k_{3-growth}[A][(36\pi)^{1/3} M_{2/3,0} - M_{0,1}]$$

$$\frac{d[L]}{dt} = -\frac{N_{sites}}{N_A} k_{4-f}[L][(36\pi)^{1/3} M_{2/3,0} - M_{0,1}] + \frac{N_{sites}}{N_A} k_{4-r} M_{0,1} - k_{1-f}[A][L] + k_{1-r}[AL]$$

$\frac{k_{1-f}}{k_{1-r}} = \frac{[AL]}{[A][L]}$ (only at time=0, $A + L \underset{k_{1-r}}{\overset{k_{1-f}}{\rightleftharpoons}} AL$ is considered to be at equilibrium)

**Initial Conditions:**

| | $[A]_0$ | $[L]_0$ | $[B]_0$ | $[AL]_0$ | $M_{i,k}$ |
|---|---|---|---|---|---|
| **Pyridine/hexanol** | 10 mM | 10 mM | 0 | 0 | 0 |
| **Pyridine/hexanol** | 10 mM | 20 mM | 0 | 0 | 0 |
| **Pyridine/hexanol** | 2.5 mM | 5 mM | 0 | 0 | 0 |
| **Toluene/hexanol** | 10 mM | 10 mM | 0 | 0 | 0 |

**Kinetic Model Parameters Estimation.** The forward and reverse reaction rate constants ($k_f$ and $k_r$, respectively) were estimated through minimizing the sum of normalized squared errors between the experiment and model for $D_{ave}$ (average diameter), and $N_p$ (concentration of the nanoparticles) using MATLAB. The sum of normalized squared errors, $J$, is given as:

$$J = \min\left( \sum_{i=1}^{\ell} \left( \frac{D_{ave}(\text{exp}) - D_{ave}(\text{model})}{D_{ave}(\text{exp})} \right)^2 + \sum_{i=1}^{\ell} \left( \frac{N_p(\text{exp}) - N_p(\text{model})}{N_p(\text{exp})} \right)^2 \right) \quad (7)$$

More details regarding the estimation of model parameters can be found in our previous publications[7, 8].

**Table S1. Model constants used to conduct the simulations.** $N_{sites}$ (number of surface sites per unit area) is obtained by averaging the number of surface sites assuming equal proportions of (111), (100) and (100) planes on the surface of the Pd nanoparticles.[9]

| Constants | Corresponding values |
|---|---|
| $N_{sites}$ | $1.26\times10^{19}$ m$^{-2}$ |
| $v_{\text{Pd}}$ | $3\times10^{-29}$ m$^3$ |
| $a_{\text{TOP}}$ | $2\times10^{-19}$ m$^2$ |

**Table S2. The extracted rate constants under different concentration of metal and ligand in pyridine.** The forward and reverse rate constants, and the corresponding normalized squared errors (*J*) obtained from fitting the in-situ SAXS data (average diameter and concentration of the nanoparticles). The rate constants summarized in the first row were used to perform simulations shown in Figures 2 and 5. Experimental conditions: $Pd(OAc)_2$ in 1:1 pyridine:hexanol, T = 100 °C.

| | $k_{1-f}$ (A+L) | $k_{1-r}$ (A+L) | $k_{2-nuc}$ | $k_{3-growth}$ | $k_{4-f}$ (B+L) | $k_{4-r}$ (B+L) | Final Size | *J* |
|---|---|---|---|---|---|---|---|---|
| | $m^3\,mol^{-1}\,h^{-1}$ | $h^{-1}$ | $h^{-1}$ | $m^3\,mol^{-1}\,h^{-1}$ | $m^3\,mol^{-1}\,h^{-1}$ | $h^{-1}$ | nm | |
| 10 mM Pd, TOP:Pd=1 | 0.043 | 0.48 | 0.010 | 16.4 | 2.15 | 37 | 4.9 | 0.14 |
| 10 mM Pd, TOP:Pd=2 | 0.025 | 0.30 | 0.018 | 25.3 | 1.51 | 38 | 4.3 | 0.09 |
| 2.5 mM Pd, TOP:Pd=2 | 0.022 | 0.25 | 0.019 | 27.3 | 1.65 | 41 | 3.3 | 0.20 |

**Table S3. The extracted rate constants in different solvent (i.e. toluene).** The forward and reverse rate constants, and the corresponding normalized squared errors (*J*) obtained from fitting the in-situ SAXS data (average diameter and concentration of the nanoparticles). Experimental conditions: $Pd(OAc)_2$ in 1:1 toluene:hexanol, T = 100 °C.

| | $k_{1-f}$ (A+L) $m^3\,mol^{-1}\,h^{-1}$ | $k_{1-r}$ (A+L) $h^{-1}$ | $k_{2-nuc}$ $h^{-1}$ | $k_{3-growth}$ $m^3\,mol^{-1}\,h^{-1}$ | $k_{4-f}$ (B+L) $m^3\,mol^{-1}\,h^{-1}$ | $k_{4-r}$ (B+L) $h^{-1}$ | Final Size nm | *J* |
|---|---|---|---|---|---|---|---|---|
| 10 mM Pd, TOP:Pd=1 | 0.011 | 0.12 | 0.13 | 1.34 | 0.04 | 0.05 | 1.6 | 0.11 |

**Table S4. The overlap of nucleation and growth for different metallic systems reported in the literature.** Estimated values for the duration of overlap between nucleation and growth (normalized to time when there is no more change in size and nanoparticle concentration), final nanoparticle diameter and polydispersity for different metallic systems, including Rh (Harada et al.[10] (without NaCl)), Pd (Mozaffari et al.[7] (pyridine and toluene, TOP:Pd=2) and Wu et al.[11] (TOP)), and Au (Chen et al.[5] ([Au(I)]=12.5 mM), Abécassis et al.[12] (acidic ligand)).

| | Length of (Nuc-Growth) $_{Overlap}$ as a % of total reaction time | Initial and Final Size (nm) | Initial and Final Polydispersity |
|---|---|---|---|
| Rh (Harada et al.[10]) | 40% | 2.0 - 2.6 | 53 - 35% |
| Pd (Mozaffari et al.[7])[a] | 30% | 2.0 - 4.3 | 22 -12% |
| Pd (Mozaffari et al.[7])[b] | 88% | 0.7 - 1.4 | 51 - 28% |
| Pd (this study) | 26% | 1.3 - 4.8 | 48 - 8% |
| Pd (Wu et al.[11]) | 25% | 2.1 - 5.5 | 40 - 11% |
| Au (Chen et al.[5]) | 12% | 2.4 - 6.0 | 21 - 9% |
| Au (Abécassis et al.[12]) | 8% | 1.5 - 7.4 | 60 - 13% |

[a] Pd synthesis in pyridine and [b] toluene

**SAXS Spectra**

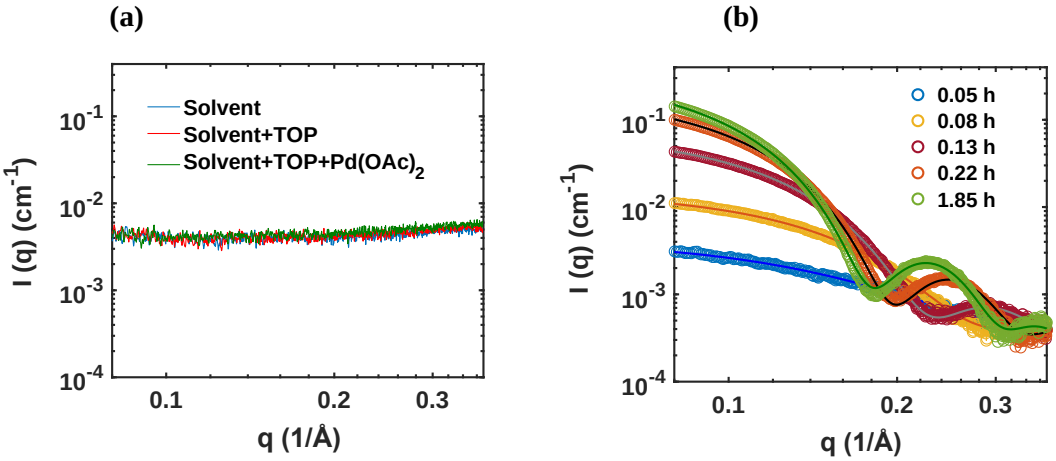


**Figure S1. Small angle x-ray spectra and fits corresponding to the synthesis of Pd nanoparticles in pyridine shown in Figure 2 in the manuscript.** (a) Background SAXS spectra for the solvent, solvent + ligand, and solvent + ligand + precursor (b) in-situ SAXS spectra after solvent subtraction and Schultz polydisperse spherical model fits at different reaction times. From bottom to top, the fitting results are 1.55 (0.0024) ± 0.35 (0.0034) nm, 2.8 (0.0013) ± 0.38 (0.0013) nm, 3.74 (0.0008) ± 0.52 (0.0011) nm, 4.5 (0.0006) ± 0.61 (0.0075) nm, and 4.93 (0.0007) ± 0.61 (0.0007) nm in diameter. The reported values in the parentheses represents the estimation of uncertainties for the SAXS fitting parameters in the parentheses were reported with 68.3 % confidence level. Experimental conditions: 10 mM $Pd(OAc)_2$ in 1:1 pyridine:hexanol, TOP:Pd=1, and T= 100 °C.

**Representative High Resolution TEM (HRTEM) Image and the Fast Fourier Transform (FFT) for the Pd Nanoparticles.**

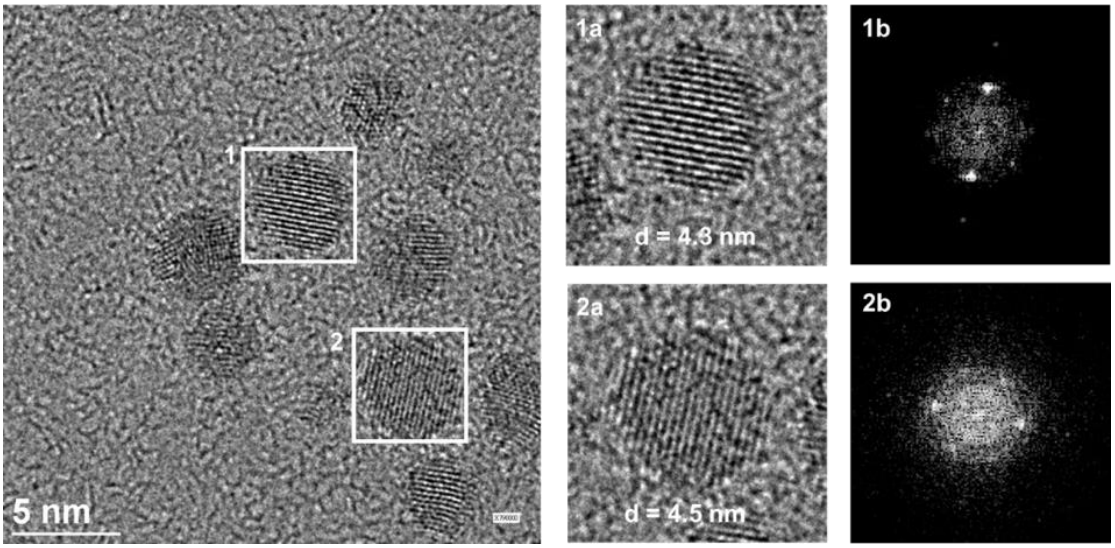


**Figure S2.** Representative high resolution TEM (HRTEM) image and the fast Fourier transform (FFT) for the Pd nanoparticles. The d-spacing of the two particles are ~ 0.23 nm which is consistent with Pd(111). Experimental conditions: 10 mM $Pd(OAc)_2$ in 1:1 pyridine/hexanol, TOP:Pd = 1, and T = 100 °C.

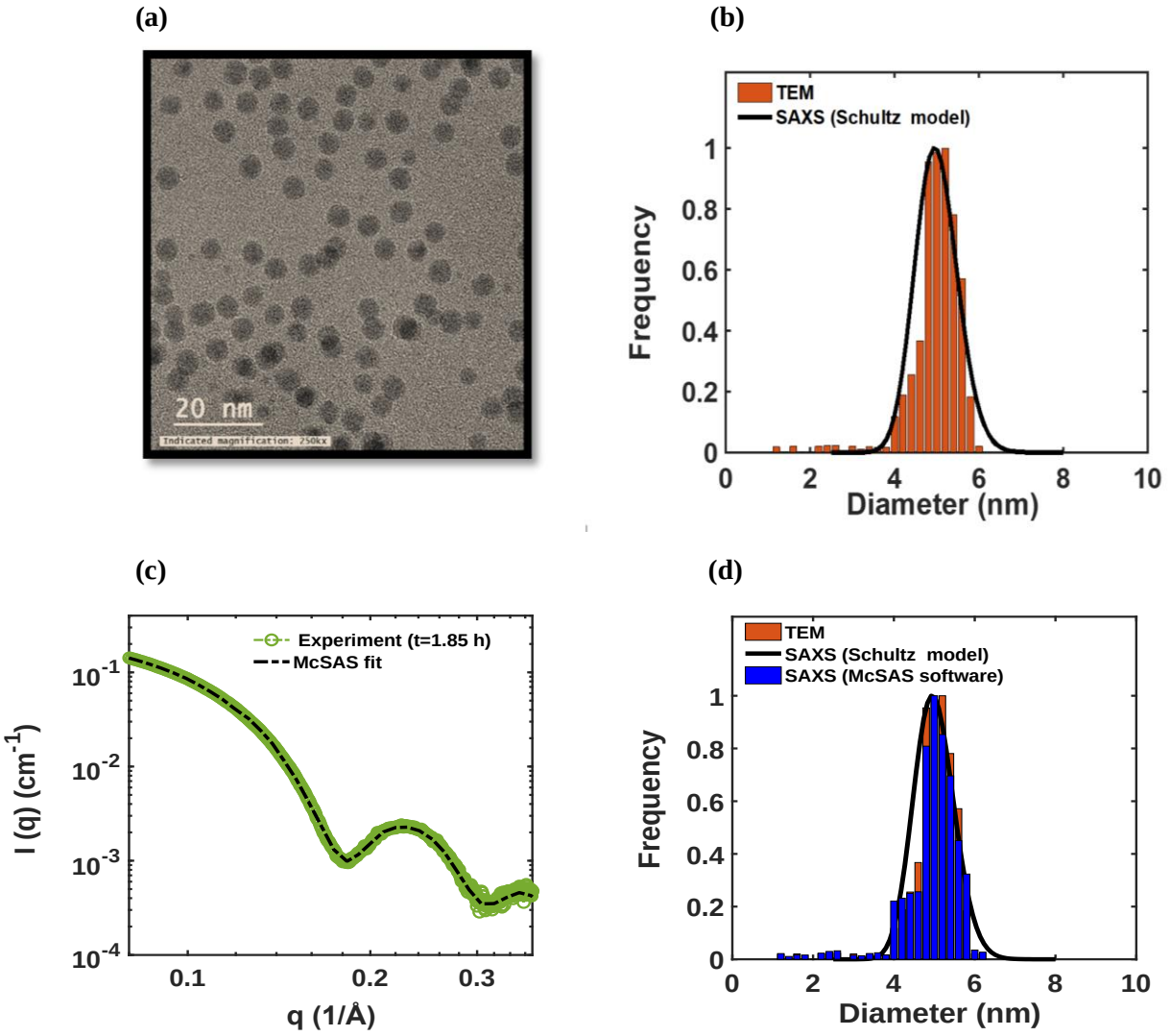


**Figure S3**. **Final Pd nanoparticle size distribution and the corresponding SAXS fitting spectra using Monte Carlo based McSAS software for synthesis in pyridine (corresponding to Figure 2 in the manuscript).** (a) Representative TEM image of Pd nanoparticles in pyridine; (b) comparing the corresponding nanoparticle size distribution obtained from TEM as obtained from measuring 500 particles (~10 images) with the one obtained from SAXS based on Shultz distribution. Based on TEM and SAXS, the average diameter in pyridine was 4.9±0.65 nm (polydispersity=13%) and 4.9±0.49 nm (polydispersity=10%), respectively.; (c) SAXS spectra fitting using McSAS software[4] at the end of reaction (the average diameter=4.8±0.70 nm; polydispersity=14%); and (d) comparing the corresponding nanoparticle size distribution obtained from Monte Carlo based McSAS software with those of the Shultz distribution model and TEM. The small percentage of smaller nanoparticles (< 4 nm) observed by TEM was also captured in the size distribution from McSAS fit. Experimental conditions: 10 mM $Pd(OAc)_2$ in 1:1 pyridine:hexanol, TOP:Pd=1, and T= 100 °C.

**Size Focusing Behavior Under Different Synthetic Conditions in Pyridine and Toluene**

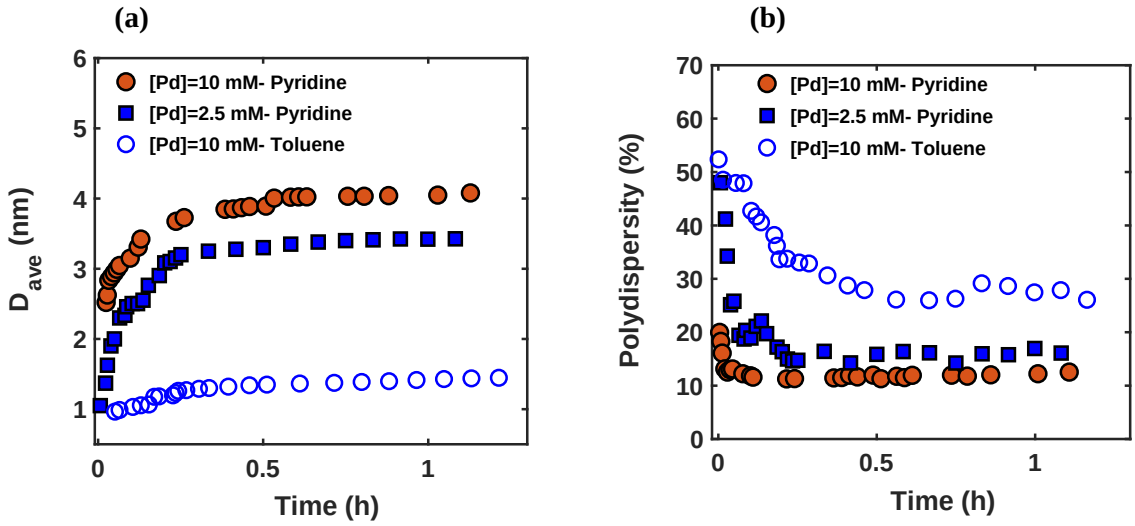


**Figure S4. In-situ SAXS data (average diameter and polydispersity) for the synthesis of Pd nanoparticles in different type of solvent and concentration.** Time evolution of (a) average diameter; and (b) polydispersity during the overlap of nucleation and growth under different synthetic conditions in pyridine (TOP:Pd=2) and toluene (TOP:Pd=1). Experimental conditions: $Pd(OAc)_2$ in 1:1 solvent/hexanol, and T = 100 °C.

**Two-Step Model (Excluding the Ligand-Metal Bindings from the Model)**

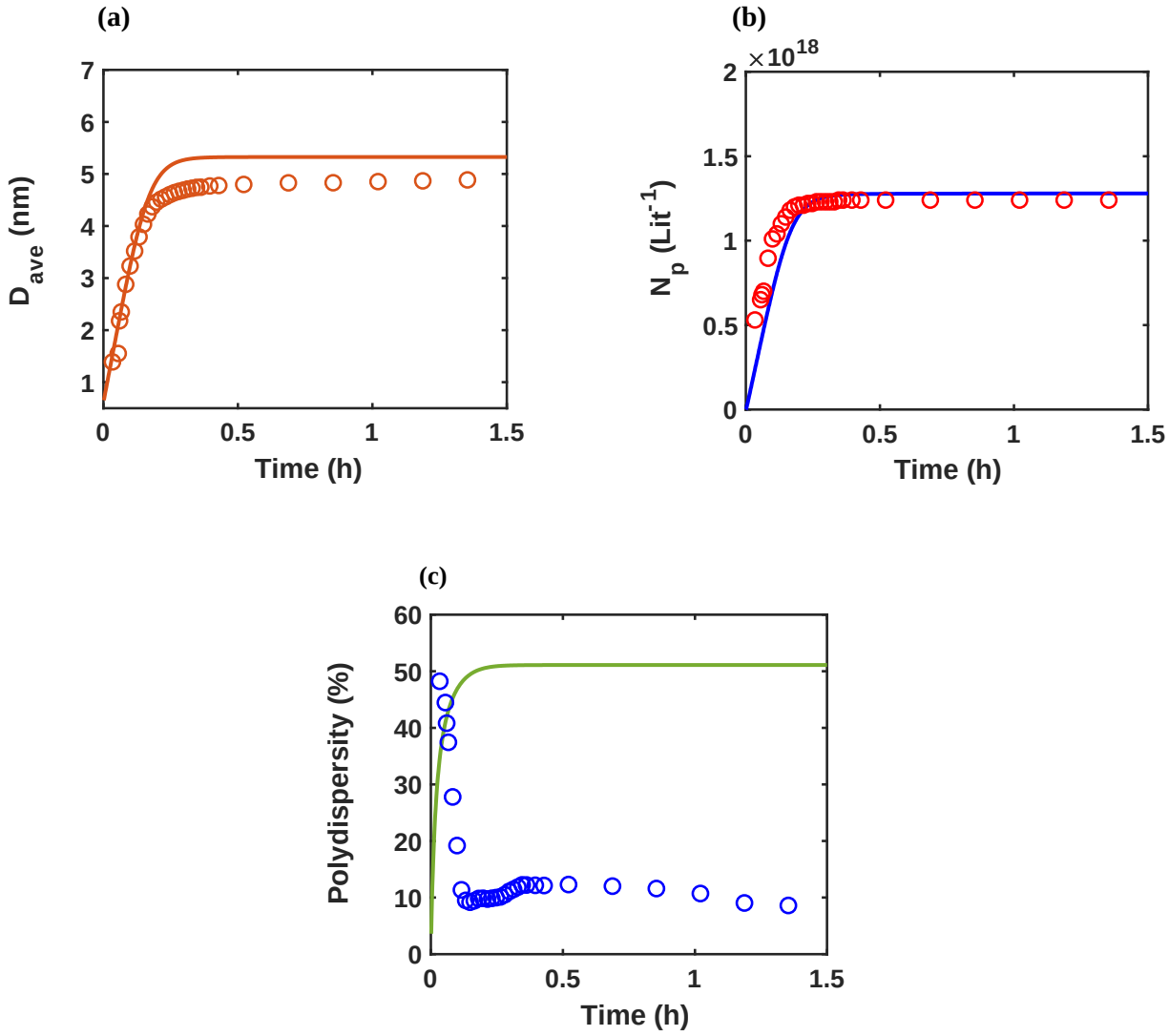


**Figure S5. Fitting the in-situ SAXS data (average diameter, concentration of nanoparticles and polydispersity) without accounting for the ligand-metal bindings.** Time evolution of (a) average diameter; (b) concentration of the nanoparticles ($N_p$); and (c) polydispersity ($P(t) = \frac{\sigma(t)}{D_{ave}(t)}$). Open circles and lines correspond to the experimental data and modeling results (excluding ligand-metal reactions), respectively. The estimated rate constants are $k_{1-nuc}$ = 0.005 $h^{-1}$ and $k_{2-growth}$ = 7.2 $m^3.mol^{-1}.h^{-1}$. Experimental conditions: 10 mM $Pd(OAc)_2$ in 1:1 pyridine:hexanol, TOP:Pd=1, and T= 100 °C.

**Growth via Monomer Addition to the Nanoparticle Surface**

$A + L \underset{k_{1\text{-}r}}{\overset{k_{1\text{-}f}}{\rightleftharpoons}} AL$ Ligand-Precursor Reversible Binding (S1)

$A \xrightarrow{k_{2\text{-}red}} P$ Reduction (S2)

$P \xrightarrow{k_{3\text{-}nuc}} B$ Nucleation (S3)

$P + B \xrightarrow{k_{4\text{-}growth}} 2B$ Growth by Monomer Addition (S4)

$B + L \underset{k_{5\text{-}r}}{\overset{k_{5\text{-}f}}{\rightleftharpoons}} BL$ Ligand-Particle Reversible Binding (S5)

**Table S5. The extracted rate constants for the case of growth via monomer addition to the nanoparticle surface.** The forward and reverse rate constants obtained from fitting in-situ SAXS data (diameter and concentration of the nanoparticles). The rate constants summarized in Table S5 were used to perform simulations shown in Figure S6. Experimental conditions: 10 mM $Pd(OAc)_2$ in 1:1 pyridine:hexanol, TOP:Pd = 1, and T = 100 °C.

| | $k_{1-f}$ (A+L) | $k_{1-r}$ (A+L) | $k_{2-red}$ | $k_{3-nuc}$ | $k_{4-growth}$ | $k_{5-f}$ (B+L) | $k_{5-r}$ (B+L) |
|---|---|---|---|---|---|---|---|
| | $m^3\,mol^{-1}\,h^{-1}$ | $h^{-1}$ | $h^{-1}$ | $h^{-1}$ | $m^3\,mol^{-1}\,h^{-1}$ | $m^3\,mol^{-1}\,h^{-1}$ | $h^{-1}$ |
| 10 mM, TOP:Pd=1 | 0.02 | 0.40 | 57.6 | 0.010 | 15.9 | 2.36 | 41.4 |

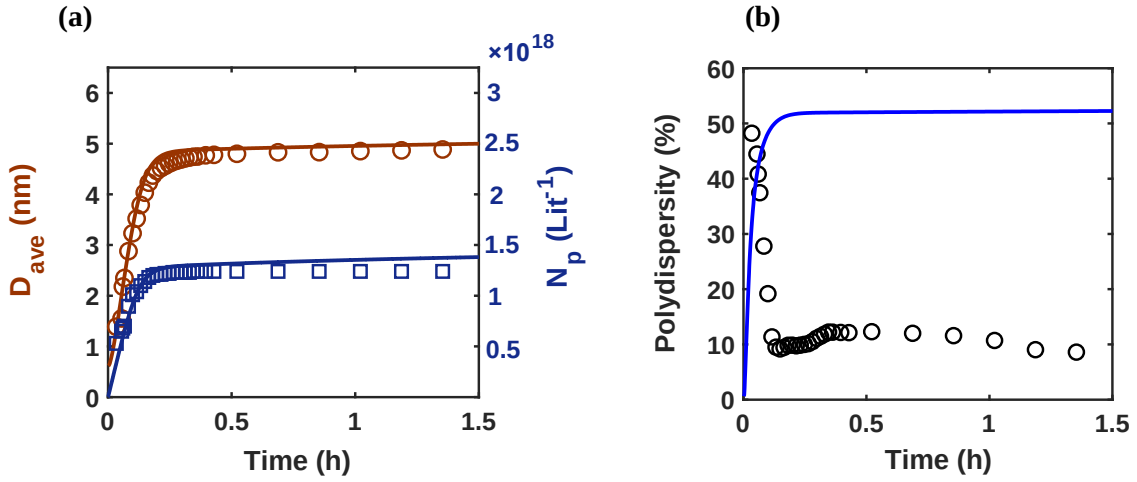


**Figure S6. Model prediction using different mode of growth (i.e. monomer addition to the nanoparticle surface) for the synthesis of Pd nanoparticles in pyridine.** Time evolution of (a) average diameter ($D_{ave}$) and concentration of the nanoparticles ($N_p$); and (b) polydispersity ($P(t) = \frac{\sigma(t)}{D_{ave}(t)}$) for the case of growth via monomer addition. Open circles and lines correspond to the experimental data from in-situ SAXS and modeling results, respectively. Experimental conditions: 10 mM $Pd(OAc)_2$ in 1:1 pyridine:hexanol, TOP:Pd=1, and T= 100 °C.

**The Time Evolution of Fractional Surface Coverage ($F_c$)**

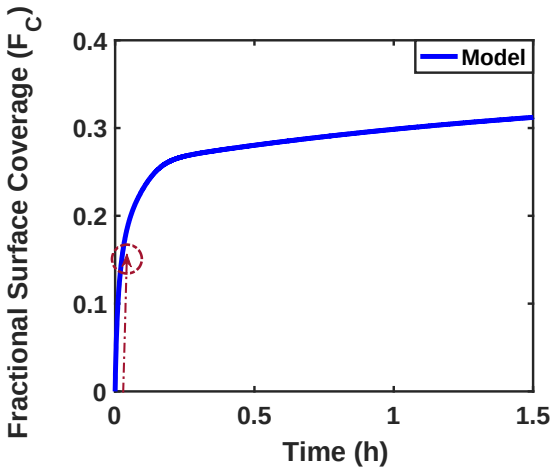


**Figure S7. The time evolution of fractional surface coverage ($F_c$).** The fractional surface coverage ($F_c$) was obtained from the fitting the in-situ data (average diameter and concentration of nanoparticles) shown in Figure 2 in the manuscript. The ligand-based model (reactions 1-4) was used to perform the simulation.

**The Sensitivity of Average Diameter and Concentration of the Nanoparticles to the Ligand-Nanoparticle Binding Rate Constants**

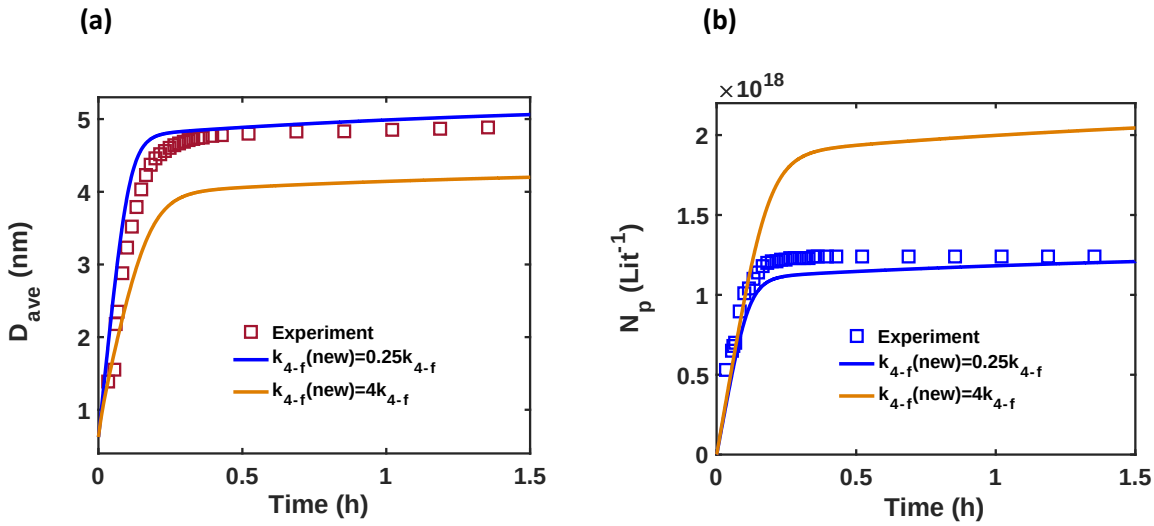


**Figure S8. Sensitivity of the model prediction to the ligand-nanoparticle binding rate constant.** The sensitivity of (a) average diameter and (b) concentration of the nanoparticles to $k_{4-f}$ (B+L) while keeping $k_{4-r}$ constant. Experimental conditions: 10 mM $Pd(OAc)_2$ in 1:1 pyridine:hexanol, TOP:Pd=1, and T= 100 °C.

# Kinetic Model Equations for the Modified PBM (Accounting for Size-Dependent Coverage)

**Moments of Size Distribution for polultations of 0.6 and 2 nm and new nuclei fomred at different reaction times**

0.6 nm population grows with time

$$\frac{dM_{0,0}}{dt} = \dot{N}_{0.6nm}$$ Nucleation rate for 0.6 nm population

$$\frac{dM_{1/3,0}}{dt} = \dot{N}_{0.6nm}(v_{0.6nm})^{1/3} + \frac{1}{3}(36\pi)^{1/3} v_{pd} N_{sites} k_{3-growth}[A][1-F_c]M_{0,0}$$ Size change rate for 0.6 nm population

$$\frac{dM_{2/3,0}}{dt} = \dot{N}_{0.6nm}(v_{0.6nm})^{2/3} + \frac{2}{3}(36\pi)^{1/3} v_{pd} N_{sites} k_{3-growth}[A][1-F_c]M_{1/3,0}$$ Area change rate for 0.6 nm population

$$\frac{dM_{1,0}}{dt} = \dot{N}_{0.6nm} v_{0.6nm} + v_{pd} N_{sites} k_{3-growth}[A][(36\pi)^{1/3} M_{2/3,0} - M_{0,1}\ ]$$ Volume change rate for 0.6 nm population

$$\frac{dM_{0,1}}{dt} = a_{TOP} N_{sites} k_{4-f}[L][(36\pi)^{1/3} M_{2/3,0} - M_{0,1}] - a_{TOP} N_{sites} k_{4-r} M_{0,1}$$ Surface coverage change rate

$$F_c = \frac{M_{0,1}}{(36\pi)^{1/3} M_{2/3,0}}$$ Fractional Surface coverage

2 nm population grows with time

$$\frac{dM_{0,0}}{dt} = \dot{N}_{2nm}$$ Nucleation rate for 2 nm population

$$\frac{dM_{1/3,0}}{dt} = \dot{N}_{2nm}(v_{2nm})^{1/3} + \frac{1}{3}(36\pi)^{1/3} v_{pd} N_{sites} k_{3-growth}[A][1-F_c]M_{0,0}$$ Size change rate for 2 nm population

$$\frac{dM_{2/3,0}}{dt} = \dot{N}_{2nm}(v_{2nm})^{2/3} + \frac{2}{3}(36\pi)^{1/3} v_{pd} N_{sites} k_{3-growth}[A][1-F_c]M_{1/3,0}$$ Area change rate for 2 nm population

$$\frac{dM_{1,0}}{dt} = \dot{N}_{2nm} v_{2nm} + v_{pd} N_{sites} k_{3-growth}[A][(36\pi)^{1/3} M_{2/3,0} - M_{0,1}\ ]$$ Volume change rate for 2 nm population

$$\frac{dM_{0,1}}{dt} = a_{TOP} N_{sites} k_{4-f}[L][(36\pi)^{1/3} M_{2/3,0} - M_{0,1}] - a_{TOP} N_{sites} k_{4-r} M_{0,1}$$ Surface coverage change rate

$$F_c = \frac{M_{0,1}}{(36\pi)^{1/3} M_{2/3,0}}$$ Fractional Surface coverage

New populations of 0.6 nm form at different reaction times and grow

$$\frac{dM_{0,0}(j)}{dt} = \dot{N}_j$$ Nucleation rate for new populations

$$\frac{dM_{1/3,0}(j)}{dt} = \dot{N}_j(v_{0.6nm})^{1/3} + \frac{1}{3}(36\pi)^{1/3} v_{pd} N_{sites} k_{3-growth}[A][1-F_c(j)]M_{0,0}(j)$$ Size change rate for new populations

$$\frac{dM_{2/3,0}(j)}{dt} = \dot{N}_j(v_{0.6nm})^{2/3} + \frac{2}{3}(36\pi)^{1/3} v_{pd} N_{sites} k_{3-growth}[A][1-F_c(j)]M_{1/3,0}(j)$$ Area change rate for new population

$$\frac{dM_{1,0}(j)}{dt} = \dot{N}_j v_{0.6nm} + v_{pd} N_{sites} k_{3-growth}[A][(36\pi)^{1/3} M_{2/3,0}(j) - M_{0,1}(j)\ ]$$ Volume change rate for new population

$$\frac{dM_{0,1}(j)}{dt} = a_{TOP} N_{sites} k_{4-f}[L][(36\pi)^{1/3} M_{2/3,0}(j) - M_{0,1}(j)] - a_{TOP} N_{sites} k_{4-r} M_{0,1}(j)$$ Surface coverage change rate

$$F_c(j) = \frac{M_{0,1}(j)}{(36\pi)^{1/3} M_{2/3,0}(j)}$$ Fractional Surface coverage

$j$=1, 2, ....200. $j$ corresponds to the new populations of 0.6 nm formed at different reaction times.

$M_{i,k} = 0$ at time=0

**Reactants Concentration**

$$\frac{d[A]}{dt} = -\frac{n_c}{N_A}\sum \dot{N} - \left(\sum \frac{N_{sites}}{N_A} k_{3-growth}[A][(36\pi)^{1/3} M_{2/3,0} - M_{0,1}]\right) - k_{1-f}[A][L] + k_{1-r}[AL]$$

$$\frac{d[AL]}{dt} = k_{1-f}[A][L] - k_{1-r}[AL]$$

$$\frac{d[B+BL]}{dt} = \frac{n_c}{N_A}\sum \dot{N} + \sum\left(\frac{N_{sites}}{N_A} k_{3-growth}[A][(36\pi)^{1/3} M_{2/3,0} - M_{0,1}]\right)$$

$$\frac{d[L]}{dt} = \sum\left(-\frac{N_{sites}}{N_A} k_{4-f}[L][(36\pi)^{1/3} M_{2/3,0} - M_{0,1}] + \frac{N_{sites}}{N_A} k_{4-r} M_{0,1}\right) - k_{1-f}[A][L] + k_{1-r}[AL]$$

$\frac{k_{1-f}}{k_{1-r}} = \frac{[AL]}{[A][L]}$ (only at time=0, $A + L \underset{k_{1-r}}{\overset{k_{1-f}}{\rightleftharpoons}} AL$ is considered to be at equilibrium)

$$M_{0,0,(tot)} = M_{0,0,(0.6nm)} + M_{0,0,(2nm)} + \sum M_{0,0}(j)$$
$$M_{1/3,0,(tot)} = M_{1/3,0,(0.6nm)} + M_{1/3,0,(2nm)} + \sum M_{1/3,0}(j)$$
$$M_{2/3,0,(tot)} = M_{2/3,0,(0.6nm)} + M_{2/3,0,(2nm)} + \sum M_{2/3,0}(j)$$
$$D_{ave} = \left(\frac{6}{p}\right)^{1/3} \frac{M_{1/3,0,(tot)}}{M_{0,0,(tot)}}$$
$$s = \sqrt{\left(\frac{6}{p}\right)^{2/3} \frac{M_{2/3,0,(tot)}}{M_{0,0,(tot)}} - \left(\frac{6}{p}\right)^{2/3} \left(\frac{M_{1/3,0,(tot)}}{M_{0,0,(tot)}}\right)^2}$$
$$P = \frac{s}{D_{ave}}$$

We note that for the modified PBM, to simulate a continuous nucleation, we generated 200 new monodisperse populations (0.6 nm in diameter) at specific times (delta function) where the concentration of nanoparticles in each additional population was chosen such that the total concentration at each time closely matches the experimental values (see schematic below and the comparison of concentration of nanoparticles for the modified PBM and full model vs. experiment in Figure S10). The number of populations (200) was chosen such that the evolution of concentration of nanoparticles is a smooth curve for the timescales considered (see the inset of Figure S10 where zoomed-in plot of the early times shows the discrete addition of nanoparticles). Therefore, in the modified PBM, the nucleation rate is constrained to closely match the concentration of the nanoparticles measured experimentally (i.e. $k_{nuc}$ is not a fitting parameter). The rate constants for growth and ligand-nanoparticle binding ($k_{growth}$ and $k_{ligand-Np}$ ) were modified/fit for different cases to investigate the effect on the evolution of size and polydispersity as described in the manuscript (i.e. (i) increasing ligand-nanoparticle binding affinity, (ii) coverage-dependent rate constant, and (iii) size-dependent rate constant).

**Schematic of Added Nanoparticles and Concentration of Nanoparticles vs. Time for the Modified PBM**

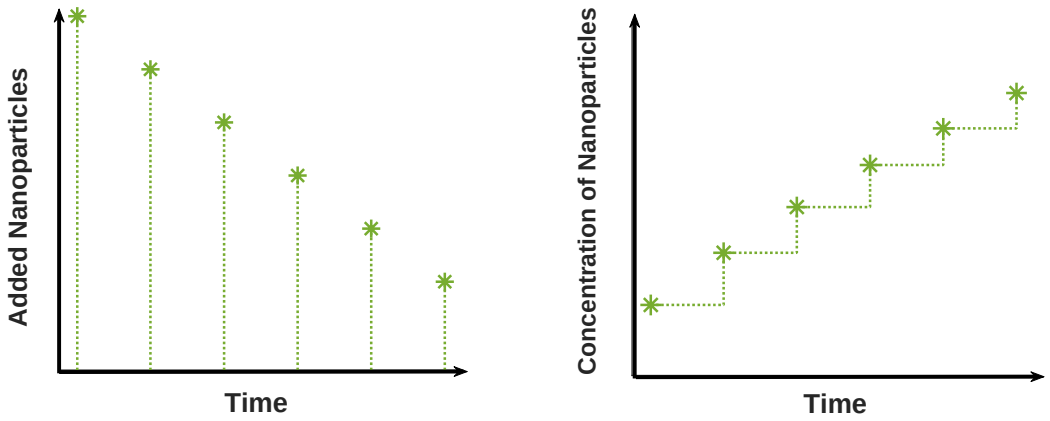

**Considering Different Initial Coverage for New-Born Nanoparticles (Nuclei).** As it is possible for the nuclei (0.6 nm) to have some (albeit low) ligand coverage, we evaluated the effect of initial nuclei surface coverage (0% and 10%) on the evolution of polydispersity (the initial ligand coverage for the 2 nm nanoparticle population is 15% in both cases). However, as shown in Figure S9, the polydispersity was almost unaffected by the higher initial ligand-coverage on the nuclei.

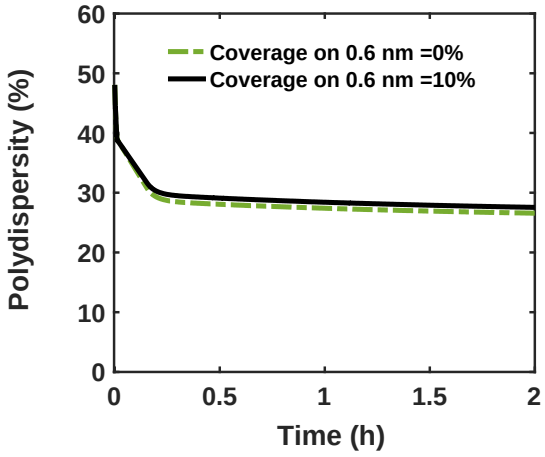


**Figure S9. The effect of initial ligand coverage on new born nanoparticles (i.e. 0.6 nm).** Time evolution of polydispersity ($P(t) = \frac{\sigma(t)}{D_{ave}(t)}$). The 0.6 nm nanoparticles have 0 and 10% ligand surface coverage at time=0 (the initial coverage of larger size population; 2 nm, is 15% in both cases). Nucleation rate (model =experiment).

**Model Prediction (Average diameter and Concentration of Nanoparticles) While Accounting for Size-Dependent Ligand Coverage**

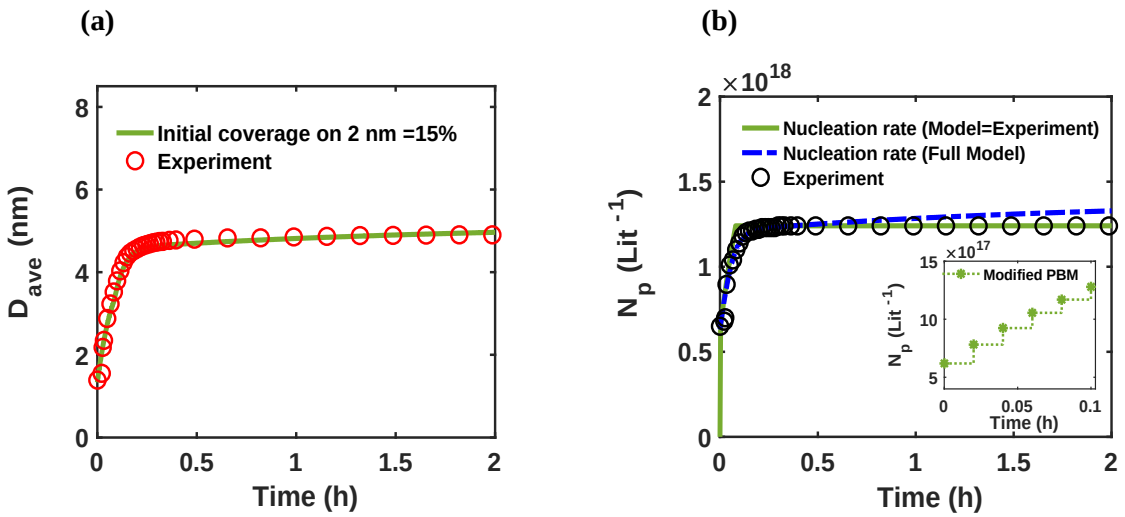


**Figure S10. Model predictions (average diameter and concentration of nanoparticles) using size-dependent ligand coverage (corresponding to Figure 5 in the manuscript).** Time evolution of (a) average diameter; (b) concentration of nanoparticles (full PBM vs. modified PBM). The 0.6 and 2 nm nanoparticles have 0% and 15% initial ligand coverage, respectively. The average diameter increases as two populations grow in size by consuming the metal precursor. The inset shows the generation of nanoparticles at few specific times (delta function) based on modified PBM (since in the original figure 200 new populations are added at different times, the line looks smooth). The rate constants summarized in Table S2 were used to perform simulations. Nucleation rate (model=experiment).

**Effects of Constant and Size-Dependent Ligand Coverage on the Evolution of Polydispersity.**

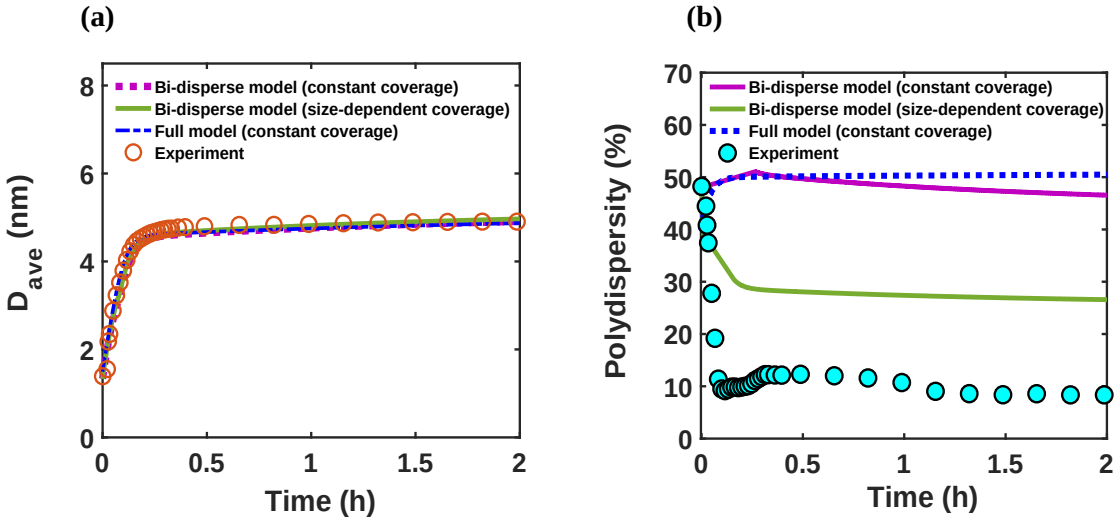


**Figure S11. Effects of constant and size-dependent ligand coverage on the evolution of polydispersity.** Time evolution of (a) average diameter and (b) polydispersity ($P(t) = \frac{\sigma(t)}{D_{ave}(t)}$). In the first case (bi-disperse model) the coverage of the entire population is constant (15%, the result did not change with the exact value of coverage). In the second case (bi-disperse model), the initial coverage on 2 nm nanoparticles is 15% and the coverage of entire population changes with time (size-dependent coverage). In the third case (full model), the coverage of entire populations is constant (ligand-nanoparticle binding is at equilibrium). In all cases the concentration of the nanoparticles is constrained to match the experiment. Experimental conditions: 10 mM $Pd(OAc)_2$ in 1:1 pyridine/hexanol, TOP:Pd = 1, and T = 100 °C.

**Effect of Continuous- vs. Burst-Nucleation on the Evolution of Polydispersity.** To investigate how much continuous nucleation and effectively the length of overlap with growth contributes to size focusing/defocusing, we compared the time evolution of the average diameter and polydispersity using different nucleation rates. To vary the nucleation rate, the number of new populations added was kept constant at 200 while the concentration of nanoparticles in each population was varied. Three different cases were evaluated: (i) no nucleation after t = 0.03 h (i.e. start with 0.6 and 2 nm nanoparticles and no additional nucleation); (ii) nucleation rate is lower than the experiment; and (iii) the nucleation rate is equal to the experiment. In case (i) where we only accounted for two populations (without any additional nucleation events), the polydispersity decreases as the two populations grow with time (see Figure S12). The decrease in polydispersity is because the percentage increase in diameter is more pronounced for the smaller nanoparticles than larger ones. For example, in the first four minutes, the smaller population grows from 0.6 to 3.5 nm, while larger nanoparticles grow from 2 to 4.7 nm despite the larger nanoparticles adding more Pd atoms to reach that size (see Figure S13). As a result, the average diameter ($D_{ave}$) increases from $1.3 \pm 0.6$ nm to $4.1 \pm 0.6$ nm and polydispersity drops from 48% to 14%. In case (ii), where the nucleation rate is lower than measured experimentally, the polydispersity drops but not to the same extent as case (i) (21% vs. 9%, respectively) because the formation of new nuclei increases the polydispersity and broadens the distribution. We note that while size focusing was observed for cases (i) and (ii), they are not experimentally representative (see final concentration of the nanoparticles compared to experiments in Figure S12). If we increase the nucleation rate to the same extent as the experimental value (i.e. case (iii)), the polydispersity drops to a lesser extent (~28%) which is far from the experimental value of ~10%. We note that the formation of new nuclei slightly lowers the average diameter (see Figure S12) but increases polydispersity.

To summarize, we investigated the effect of nucleation rate and length of overlap with growth, on the evolution of polydispersity. The results for different nucleation rates confirm that continuous nucleation contributes to defocusing of the size distribution.

**Effect of Nucleation Rate on the Evolution of Size Distribution**

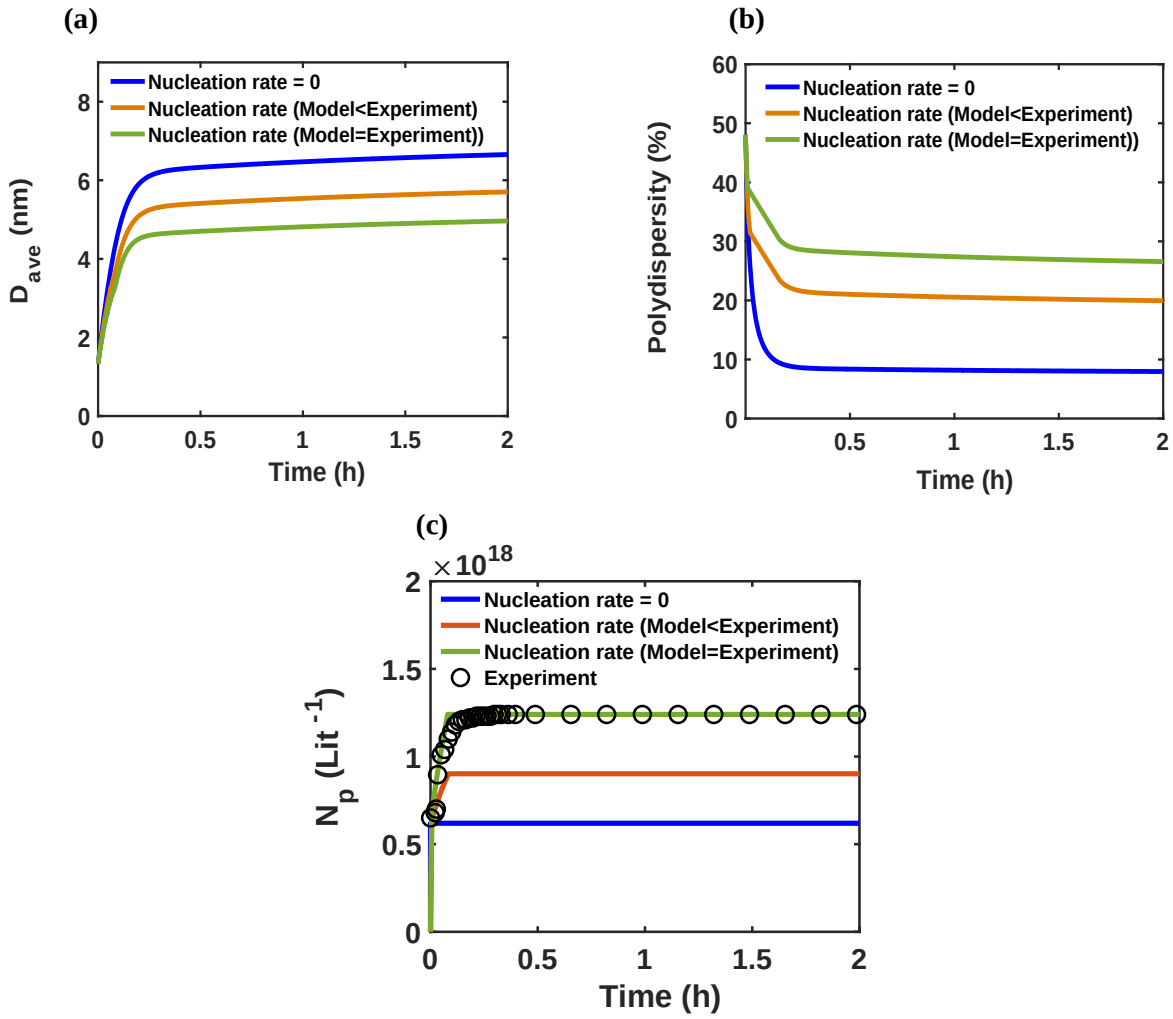


**Figure S12. The effect of nucleation rate on the evolution of size distribution.** Time evolution of (a) average diameter; (b) polydispersity ($P(t) = \frac{\sigma(t)}{D_{ave}(t)}$); and (c) concentration of nanoparticles with and without nucleation events. The 0.6 and 2 nm nanoparticles have 0% and 15% initial ligand coverage, respectively. The average diameter increases as two populations grow in size by consuming the metal precursor. Three different cases were considered: (i) Nucleation rate (model)=0; (ii) Nucleation rate (model < experiment); and (iii) Nucleation rate (model = experiment). Note that at time=0, the total concertation of nanoparticles (which includes both 0.6 and 2 nm populations) is $0.62\times10^{+18}$ $Lit^{-1}$.

**Comparison of the Growth of Two Different Size Populations as a Function of Time for the Case of Size-Dependent Ligand Coverage.** In this case, the 0.6 and 2 nm nanoparticles have 0% and 15% initial ligand coverage, respectively. The average diameter increases as two populations grow in size by consuming the metal precursor (no additional nucleation event takes place).

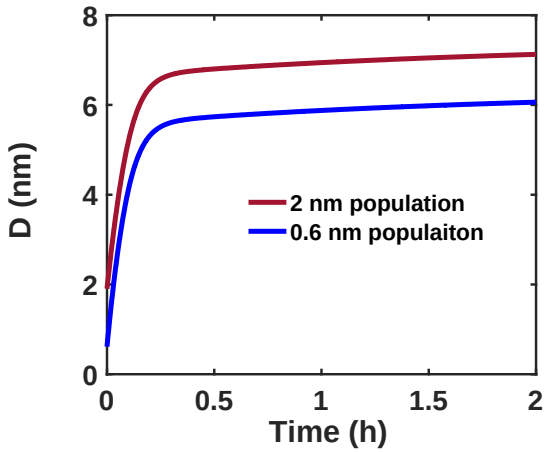


**Figure S13. Comparison of the growth of two different size populations.** The metal precursor and ligands are shared among 0.6 nm (new born nanoparticles) and 2 nm nanoparticles. The 0.6 and 2 nm nanoparticles have 0% and 15% initial ligand coverage, respectively. The rate constants shown in Table S2 were used to perform simulations. Nucleation rate (model)=0.

**Effect of Ligand-Nanoparticle Binding Affinity on the Evolution of Polydispersity.** To alter the initial coverage on 2 nm nanoparticles from 15-40% (i.e. stronger ligand-nanoparticle affinity), the $k_{4-f}$ (B+L) shown in Table S2 changed by 1.5-3.5 times while keeping $k_{4-r}$ constant (this results in $K_{4\text{-eq}}$ to increase by 1.5-3.5 times).

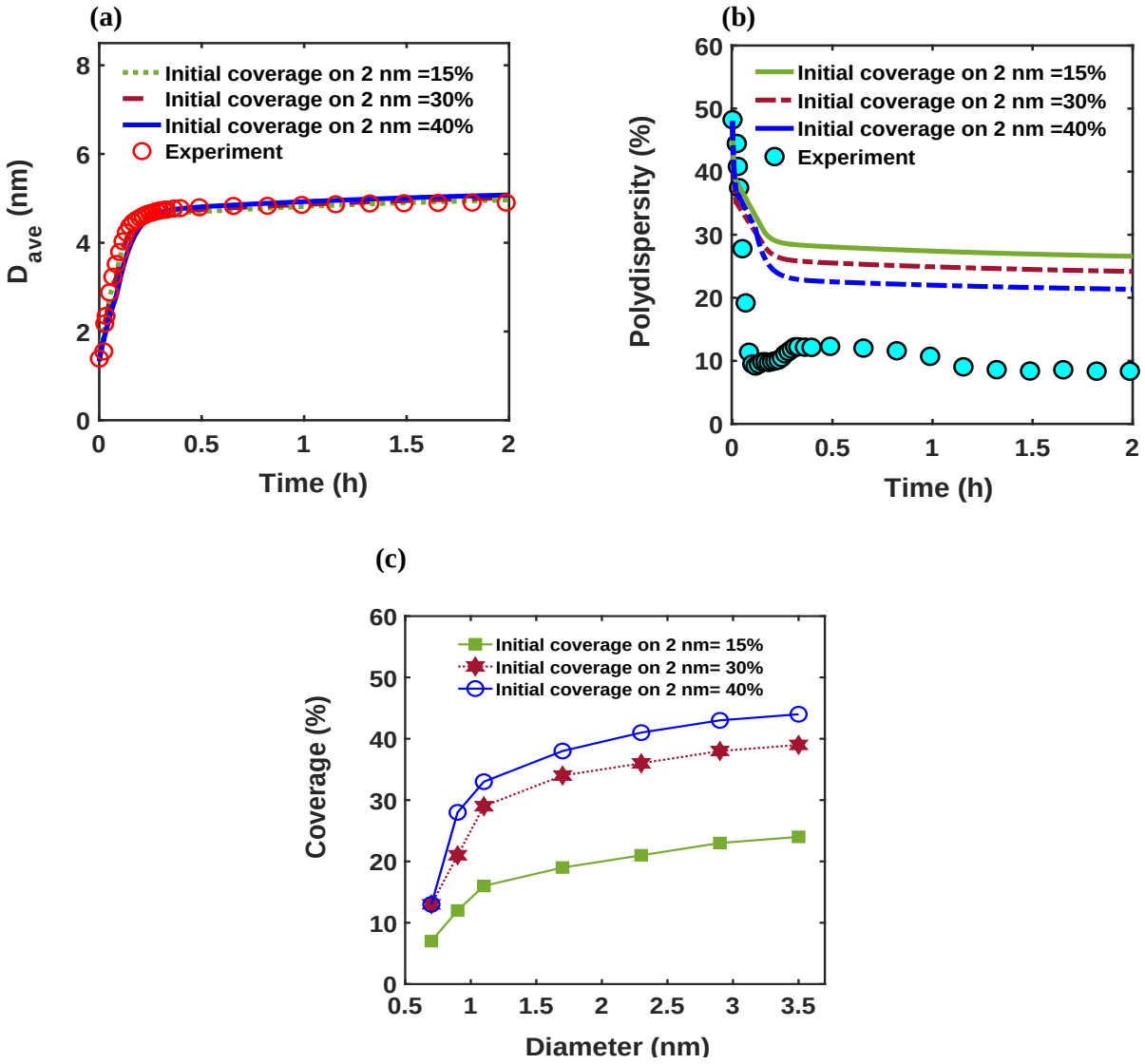


**Figure S14. The effect of ligand-nanoparticle binding affinity on the evolution of polydispersity and coverage of different size nanoparticles (corresponding to Figure 6 in the manuscript).** Time evolution of (a) average diameter and (b) polydispersity ($P(t) = \frac{\sigma(t)}{D_{ave}(t)}$); and (c) coverage as a function of diameter at different initial ligand coverage of larger size population at time=0.11 h. In the first case, the 2 nm nanoparticles have 15% initial ligand coverage, while in the second and third case, the 2 nm nanoparticles have 30 and 40% ligand surface coverage at time=0 (the initial coverage of smaller size population; 0.6 nm,

is zero in all cases). The maximum coverage for the cases with 15%, 30%, and 40% initial coverage on 2 nm nanoparticles is 32%, 45%, and 55%, respectively. Nucleation rate (model = experiment).

**Effect of High Ligand Coverage on the Evolution of Polydispersity.** It is important to note that regardless of considering any initial coverage on the 2 nm nanoparticles, the larger nanoparticles have higher surface coverage than the smaller ones (see Figure S14c) due to the gradual increase of coverage on the nanoparticle surface with time. If the 2nm nanoparticles have a much higher initial coverage of 80% (maximum coverage reaches 95%, corresponding to a much higher metal-ligand affinity ($k_{4-f}$ (B+L), 7 times the value shown in Table S2), the polydispersity dropped to the experimental value of 10%, however, the model failed to capture the evolution of average diameter as a result of fast surface capping (low concentration of surface sites is available for growth) which leads to much slower growth rate (see Figure S15).

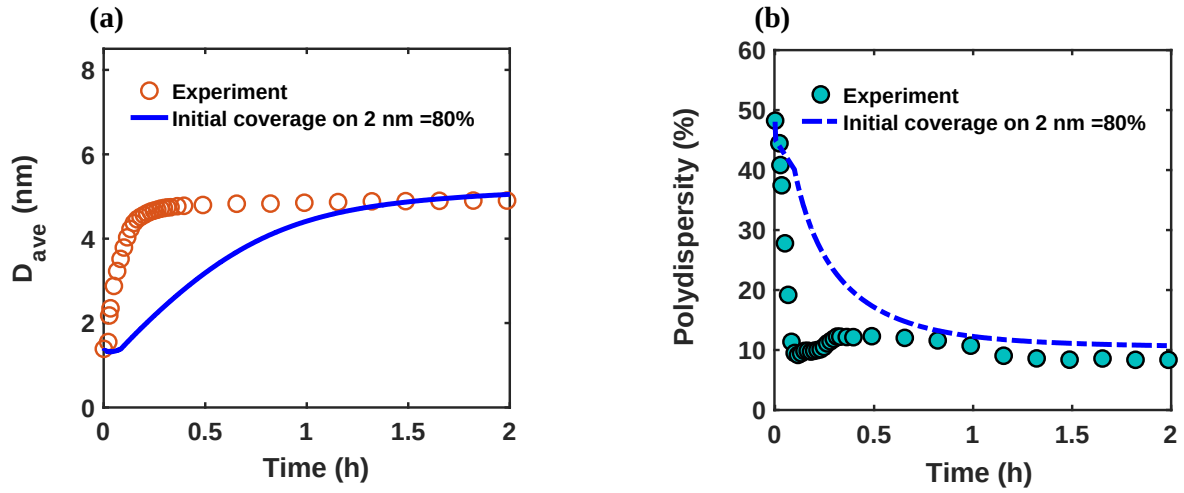


**Figure S15. Effect of high ligand coverage on the evolution of polydispersity without altering the growth rate constant.** Time evolution of (a) average diameter; and (b) polydispersity ($P(t) = \frac{\sigma(t)}{D_{ave}(t)}$) with 80% initial ligand coverage for 2 nm (larger size) population (the initial ligand coverage for the 0.6 nm nanoparticle is zero). The maximum coverage reaches 95%. Nucleation rate (model = experiment). $k_{1-f}$ (A+L)=0.043 $m^3\,mol^{-1}\,h^{-1}$, $k_{1-r}$ (A+L)=0.48 $h^{-1}$, $k_{3-growth}$=16.4 $m^3\,mol^{-1}\,h^{-1}$, $k_{4-f}$ (B+L)=15 $m^3\,mol^{-1}\,h^{-1}$, $k_{4-r}$ (B+L)=37 $h^{-1}$.

**Effect of High Ligand Coverage on the Evolution of Polydispersity While Adjusting $k_{3-growth}$).** To capture the size evolution shown in Figure S16, $k_{3-growth}$ increased by 2 times and $k_{4-f}$ (B+L) shown in Table S2 increased by 7 times. While adjustment of k's helped with capturing the size evolution, it could not capture the polydispersity from the experiment. The final polydispersity for this case (95% maximum coverage) was similar to the prediction of polydispersity shown in Figure S14 once the maximum coverage was 55% (for coverage of 95% and 55%, the predicted polydispersity was 20 and 22%, respectively).

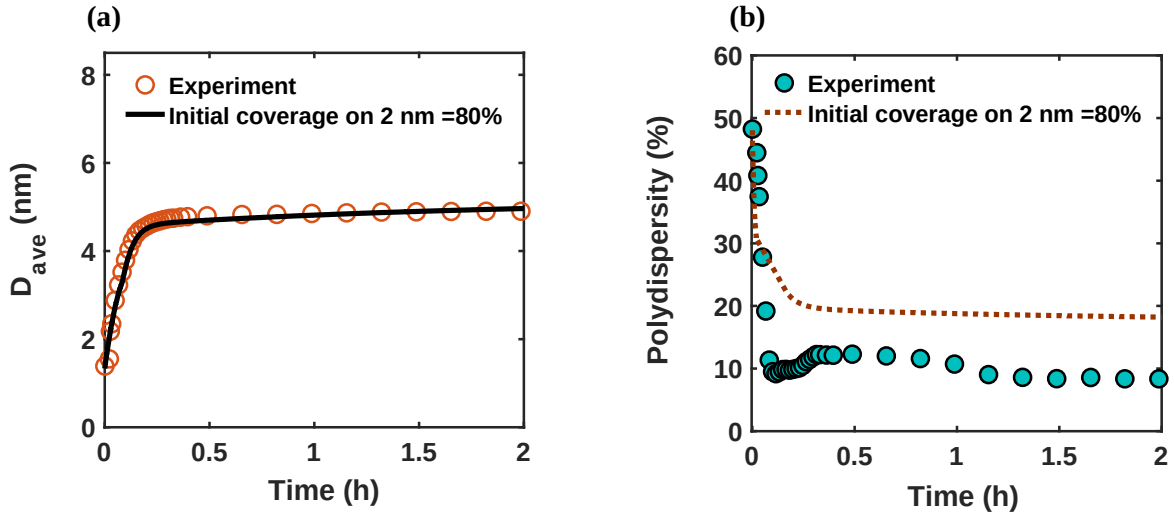


**Figure S16. Effect of high ligand coverage on the evolution of polydispersity while altering the growth rate constant.** Time evolution of (a) average diameter; and (b) polydispersity ($P(t) = \frac{\sigma(t)}{D_{ave}(t)}$) with 80% initial ligand coverage for 2 nm (larger size) population (the initial ligand coverage for the 0.6 nm nanoparticle is zero). The maximum coverage reaches 95%. Nucleation rate (model = experiment). $k_{3-growth}$ is adjusted in this case. $k_{1-f}$ (A+L)=0.043 $m^3\,mol^{-1}\,h^{-1}$, $k_{1-r}$ (A+L)=0.48 $h^{-1}$, $k_{3-growth}$=32.8 $m^3\,mol^{-1}\,h^{-1}$, $k_{4-f}$ (B+L)=15 $m^3\,mol^{-1}\,h^{-1}$, $k_{4-r}$ (B+L)=37 $h^{-1}$.

**Model Predictions for the Case of Coverage-Dependent Growth Rate Constant Using Different Combination of Bi-Disperse Nanoparticles in Pyridine**

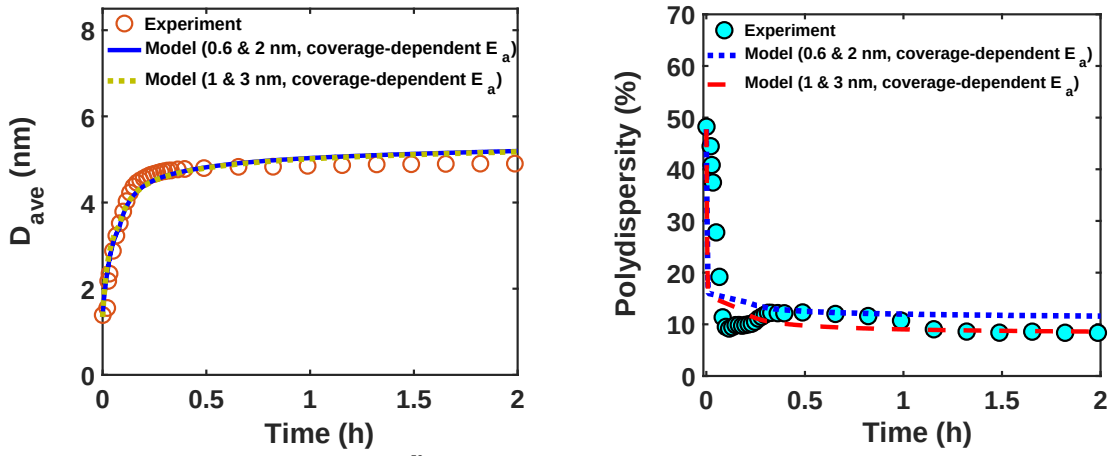


**Figure S17. Model predictions for the case of coverage-dependent growth rate constant using different combination of bi-disperse nanoparticles (0.6 and 2 nm vs. 1 and 3 nm) and comparing the effects on the evolution of polydispersity.** Time evolution of (a) average diameter and (b) polydispersity ($P(t) = \frac{\sigma(t)}{D_{ave}(t)}$). Experimental conditions: 10 mM $Pd(OAc)_2$ in 1:1 pyridine/hexanol, TOP:Pd = 1, and T = 100 °C.

**Coverage-Dependent Growth Rate Constant**

**Estimation of $C_L$ and $C_g$.** $C_L$ and $C_g$ in the following equations:

(i) $\Delta H_L(\theta) = \Delta H_{0-L}(1 - C_L\theta)$ and (ii) $\Delta H_G(\theta) = \Delta H_{0-G}(1 - C_g\theta)$ were extracted from the linear decay in adsorption energy using the initial and final data points shown in Figure 7, i.e. ~0 and 20% coverage.

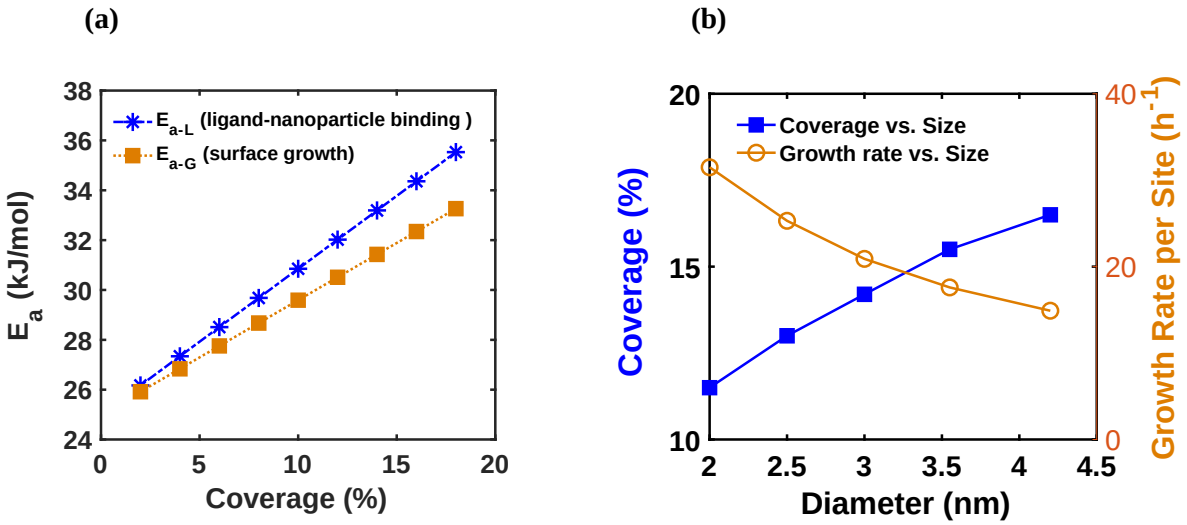


**Figure S18. Coverage and growth rate prediction for the case of coverage-dependent growth rate constant.** Model prediction of (a) $E_{a-L}$ (ligand-nanoparticle binding) and $E_{a-G}$ (surface growth) as a function of coverage (corresponding to Figure 8 in the main manuscript) and (b) coverage (blue square) and growth rate per site (orange circle) both as a function of diameter at time=0.15 h (growth rate constant decreases with coverage and growth is normalized to the concentration of surface sites). The ligand surface coverage affects both the enthalpy and activation energies for ligand-nanoparticle binding and surface growth ($\Delta H_{0-L}$=−260 kJ/mol, $E_{a-L0}$=25 kJ/mol; $\Delta H_{0-G}$ =−340 kJ/mol, $E_{a-G0}$=25 kJ/mol, all reported values are at zero coverage).

**Model Predictions for the Case of Coverage Dependent and Independent Growth Rate Constant**

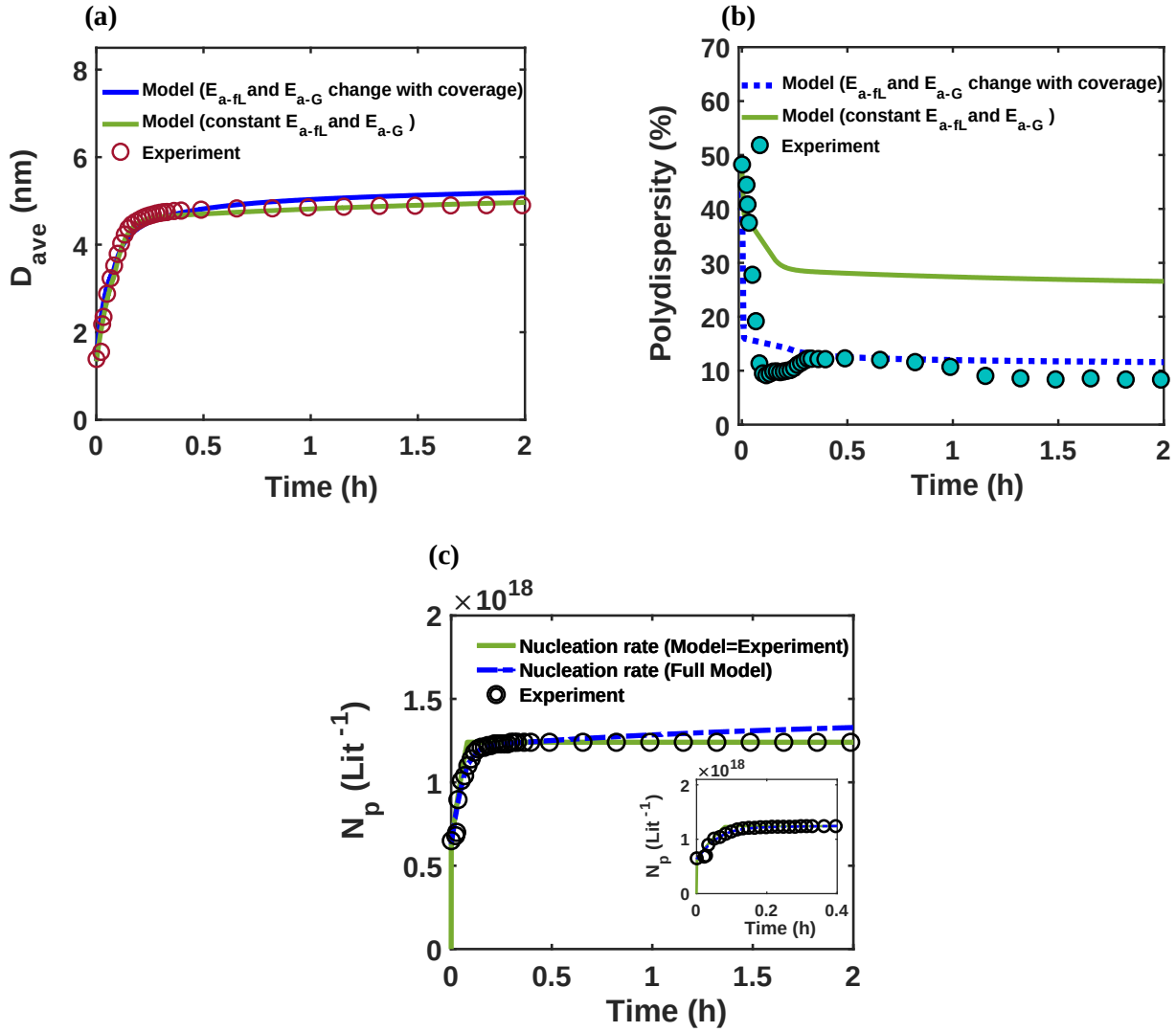


**Figure S19. Model predictions for the case of coverage dependent and independent growth rate constant.** Time evolution of (a) average diameter; (b) polydispersity ($P(t) = \frac{\sigma(t)}{D_{ave}(t)}$) for two different cases; and (c) concentration of nanoparticles (modified PBM vs. full model). In the first case, the 2 nm nanoparticles have 15% initial ligand coverage and the activation energies are not affected by coverage (the initial coverage of smaller size population; 0.6 nm, is zero in all cases). In the second case, the 2 nm nanoparticles have 15% ligand surface coverage at time=0 and the surface coverage affects both the enthalpy and activation energies for ligand-nanoparticle binding and surface growth ($\Delta H_{0-L}$=−260 kJ/mol, $E_{a-L0}$=25 kJ/mol; $\Delta H_{0-G}$ =−340 kJ/mol, $E_{a-G0}$=25 kJ/mol, all reported values are at zero coverage).

**Model Predictions for the Case of Coverage-Dependent Growth Rate Constant Under Different Metal Concentration in Pyridine**

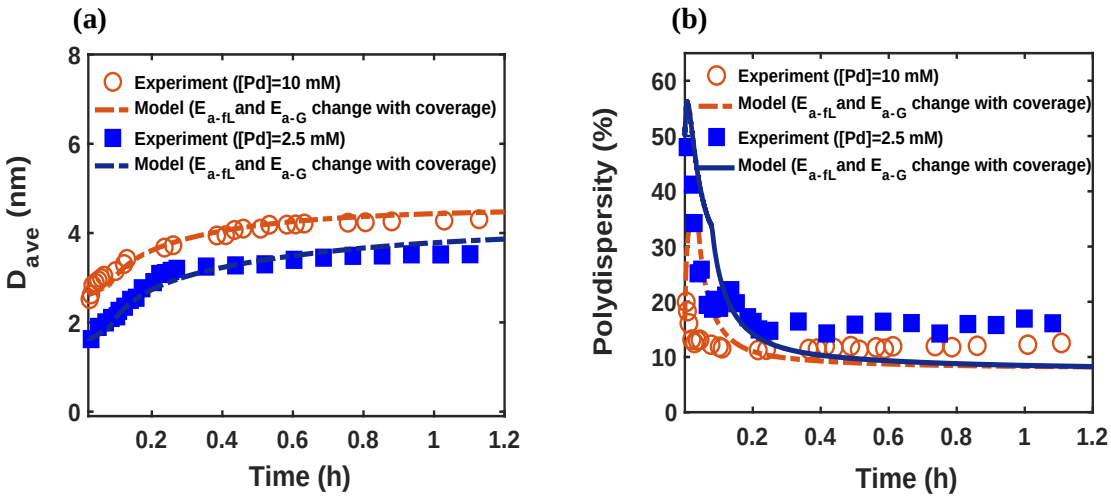


**Figure S20. Model predictions for the case of coverage-dependent growth rate constant under different metal concentration in pyridine.** Time evolution of (a) average diameter; (b) polydispersity ($P(t) = \frac{\sigma(t)}{D_{ave}(t)}$) under different synthetic conditions. Here, the 2.5 nm nanoparticles have 15% ligand surface coverage at time=0 (the initial coverage of smaller size population; 0.6 nm, is zero in all cases) and the surface coverage affects both the enthalpy and activation energies for ligand-nanoparticle binding and surface growth ($\Delta H_{0-L}$=−260 kJ/mol, $E_{a-L0}$=25 kJ/mol; $\Delta H_{0-G}$ =−340 kJ/mol, $E_{a-G0}$=25 kJ/mol, all reported values are at zero coverage). Experimental conditions: 2.5 and 10 mM $Pd(OAc)_2$ in 1:1 pyridine:hexanol, TOP:Pd=2, and T= 100 °C.

**Table S6. The extracted rate constants under different concentration of metal and ligand in pyridine for the case of coverage-dependent growth rate constant.** The estimated rate constants to capture the evolution of average diameter, polydispersity, and concentration of nanoparticles in pyridine. The rate constants shown in Table S6 were used to perform simulations shown in Figure S20. Experimental conditions: $Pd(OAc)_2$ in 1:1 pyridine:hexanol, T= 100 °C.

| | $k_{1-f}$ (A+L) | $k_{1-r}$ (A+L) | $k_{3-growth}$ | $k_{4-f}$ (B+L) | $k_{4-r}$ (B+L) |
|---|---|---|---|---|---|
| | $m^3\,mol^{-1}\,h^{-1}$ | $h^{-1}$ | $m^3\,mol^{-1}\,h^{-1}$ | $m^3\,mol^{-1}\,h^{-1}$ | $h^{-1}$ |
| 10 mM Pd, TOP:Pd=1 | 0.043 | 0.48 | 70 | 3.75 | $0.003\times10^{-4}$ |
| 10 mM Pd, TOP:Pd=2 | 0.025 | 0.30 | 77 | 3.75 | $0.003\times10^{-4}$ |
| 2.5 mM Pd, TOP:Pd=2 | 0.022 | 0.25 | 99 | 3.75 | $0.003\times10^{-4}$ |

**Model Predictions for the Case of Coverage-Dependent Growth Rate Constant in a Different Solvent Type (i.e. Toluene).** Regarding the different kinetics of nucleation and growth in toluene vs. pyridine, we note that the nucleation and growth kinetics will be affected not only by the ligand-nanoparticle binding but also the nature of pre-reduction complex. Unlike toluene, pyridine is a coordinating solvent and can bind with the metal precursor and form a different pre-reduction complex. The difference in the nature of pre-reduction complex in toluene and pyridine affects the reactivity which results in different nucleation and growth kinetics. With respect to the size focusing in toluene, we note that experimentally we observe size focusing (55% down to 30%). Additionally, using the same coverage effect on activation energy of growth in toluene as in pyridine, we observe a size focusing from the model. While the model overestimates the size focusing, we note that for such small nanoparticles, 30% experimental (1.5 ± 0.45 nm) vs. 15% from the model (1.5 ± 0.22 nm), the difference is not that large. It is likely that the coverage effect is solvent dependent since solvents have been shown to affect coverage of ligands and final nanoparticle size[11, 12]. However, this is beyond the scope of this work.

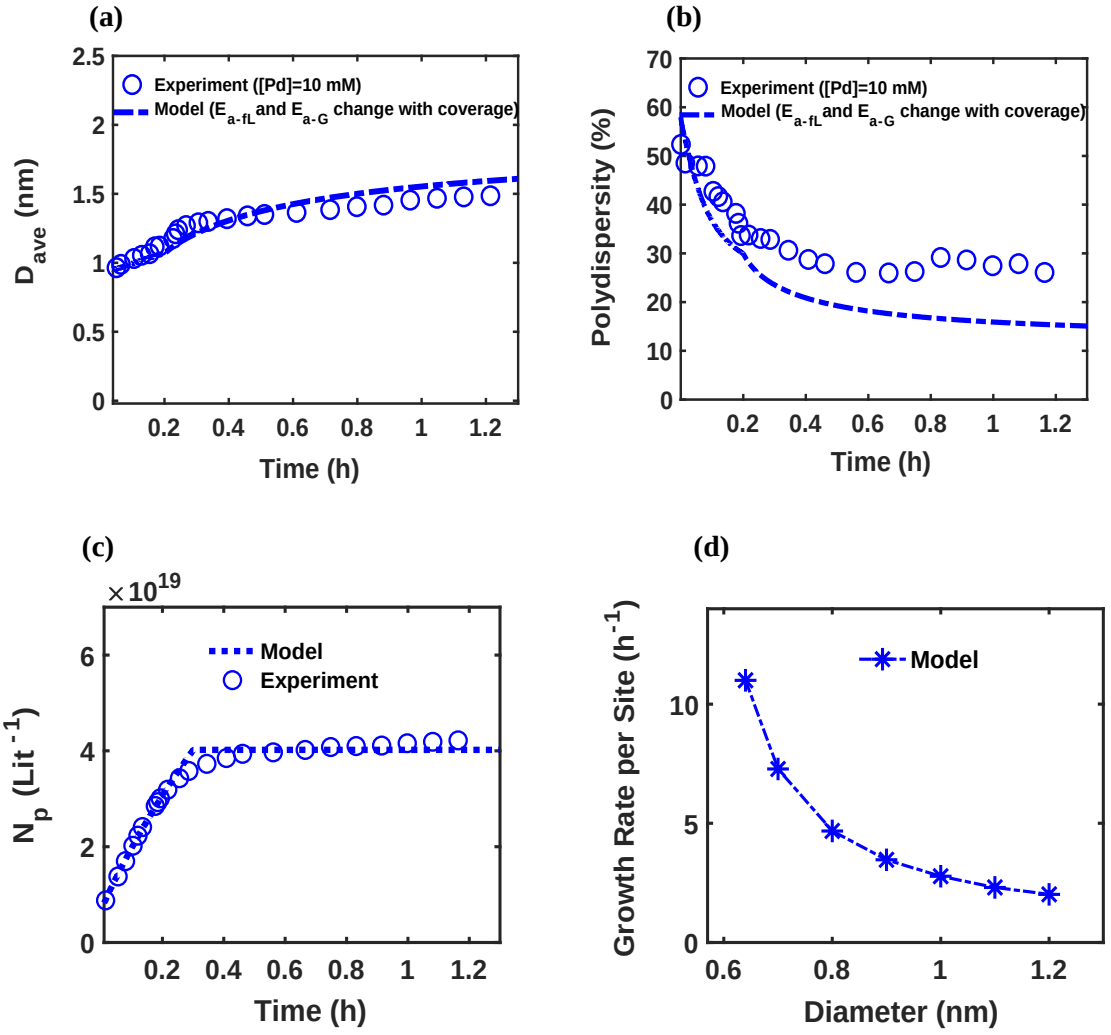


**Figure S21. Model predictions for the case of coverage-dependent growth rate constant in different type of solvent (i.e. toluene).** Time evolution of (a) average diameter; (b) polydispersity ($P(t) = \frac{\sigma(t)}{D_{ave}(t)}$) under different synthetic conditions; (c) concentration of nanoparticles; and (d) growth rate as a function of

diameter. Here, the 1.5 nm nanoparticles have 5% ligand surface coverage at time=0 (the initial coverage of smaller size population; 0.6 nm, is zero in all cases). and the surface coverage affects both the enthalpy and activation energies for ligand-nanoparticle binding and surface growth ($\Delta H_{0-L} = -260$ kJ/mol, $E_{a-L0}$=25 kJ/mol; $\Delta H_{0-G} = -340$ kJ/mol, $E_{a-G0}$=25 kJ/mol, all reported values are at zero coverage). Experimental conditions: 10 mM $Pd(OAc)_2$ in 1:1 toluene:hexanol, TOP:Pd=1, and T= 100 °C.

**Table S7. The extracted rate constants in different solvent (i.e. toluene) for the case of coverage-dependent growth rate constant.** The estimated rate constants to capture the evolution of average diameter, polydispersity, and concentration of nanoparticles in toluene. The rate constants shown in Table S6 were used to perform simulations shown in Figure S21. Experimental conditions: $Pd(OAc)_2$ in 1:1 toluene:hexanol, T= 100 °C.

| | $k_{1-f}$ (A+L) | $k_{1-r}$ (A+L) | $k_{3-growth}$ | $k_{4-f}$ (B+L) | $k_{4-r}$ (B+L) |
|---|---|---|---|---|---|
| | $m^3\,mol^{-1}\,h^{-1}$ | $h^{-1}$ | $m^3\,mol^{-1}\,h^{-1}$ | $m^3\,mol^{-1}\,h^{-1}$ | $h^{-1}$ |
| 10 mM Pd, TOP:Pd=1 | 0.01 | 0.13 | 2.5 | 0.4 | $0.005\times10^{-6}$ |

**Growth via Monomer Addition to the Nanoparticle Surface**

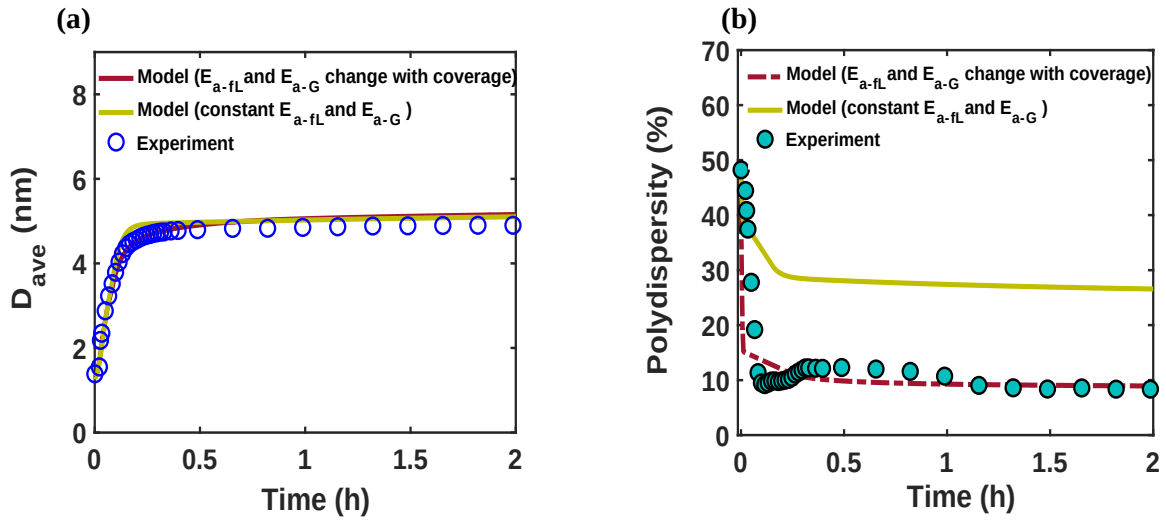


**Figure S22. Model predictions for the case of coverage-dependent growth rate constant using different growth mode (i.e. monomer addition to the nanoparticle surface).** Time evolution of (a) average diameter; (b) polydispersity ($P(t) = \frac{\sigma(t)}{D_{ave}(t)}$) for two different cases. In the first case, the 2 nm nanoparticles have 15% initial ligand coverage and the activation energies are not affected by coverage (the initial coverage of smaller size population; 0.6 nm, is zero in all cases). In the second case, the 2 nm nanoparticles have 15% ligand surface coverage at time=0 and the surface coverage affects both the enthalpy and activation energies for ligand-nanoparticle binding and surface growth ($\Delta H_{0-L}$=−260 kJ/mol, $E_{a-L0}$=25 kJ/mol; $\Delta H_{0-G}$ =−340 kJ/mol, $E_{a-G0}$=25 kJ/mol, all reported values are at zero coverage. Nucleation rate (model = experiment). Experimental conditions: 10 mM $Pd(OAc)_2$ in 1:1 pyridine:hexanol, TOP:Pd=1, and T= 100 °C.

**Effect of Nanoparticle Size on the Enthalpy of Surface Growth**

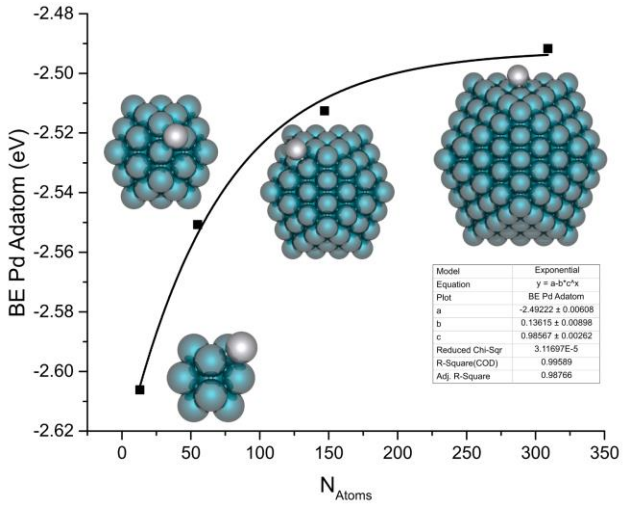


**Figure S23. Enthalpy of growth.** The binding energy of a Pd adatom (on hollow position in every case) on Pd nanoparticles of different sizes (ranging from 10-300 atoms) using the Square Root Bond cutting model[16] applied on predicting the stability of metal nanoparticles[17].

**Size-Dependent Growth and Ligand-Nanoparticle Binding Rate Constants**

In our model, we assumed that enthalpy of ligand-nanoparticle binding ($\Delta H_L$) follows the same trend as the enthalpy of growth ($\Delta H_G$ ) shown in Figure S23. For the 2 nm nanoparticles, we used $\Delta H_{0-L}$=−260 kJ/mol (which is similar to the value obtained from Pd(111) DFT calculations shown in Figure 7) and $E_{a-L0}$=25.3 kJ/mol; and then we estimated the $\Delta H_L$ and $E_{a-L}$ value for the smaller nanoparticles (i.e. more exothermic). Regarding the growth enthalpy, for the 0.6 nm nanoparticles, we used $\Delta H_{0-G}$=−251 kJ/mol (as shown in Figure S23) and $E_{a-G0}$=25.3 kJ/mol; and then we estimated the $\Delta H_G$ and $E_{a-G}$ values for the larger nanoparticles using the trend shown in Figure S23. Note that the $\Delta H_L$ and $\Delta H_G$ remain constant once the nanoparticle size gets larger than 2 nm and this has been considered in our model. The values of $\alpha_L$ and $\alpha_G$ are 0.3 similar to the case of coverage-dependent growth rate constant.

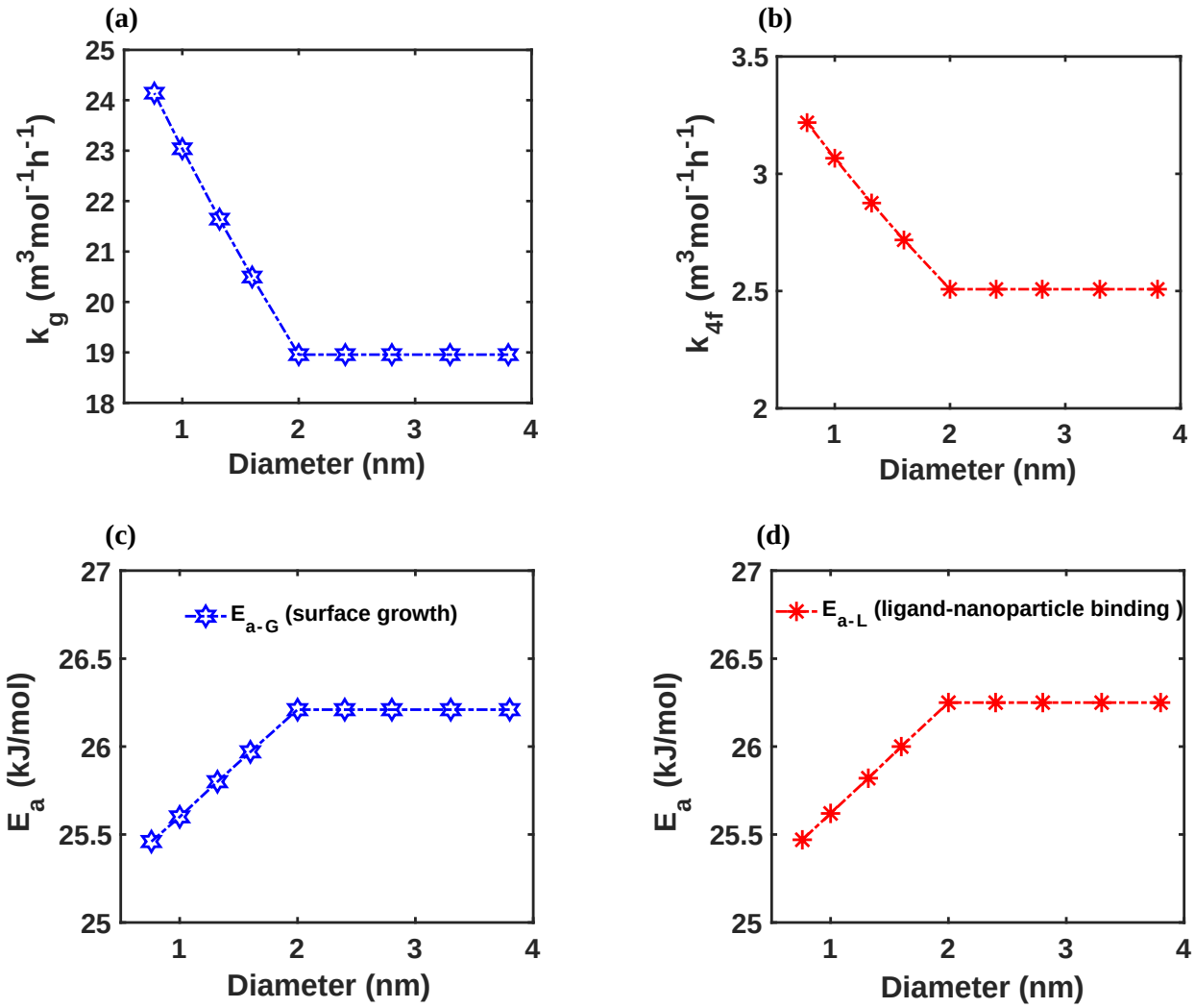


**Figure S24. The effect of nanoparticle diameter on growth and ligand-nanoparticle binding rate constants (corresponding to Figure S25).** The rate constants for (a) surface growth ($k_g$); and (b) ligand-nanoparticle binding constant ($k_{4-f}$) both as a function of diameter at time=0.10 h; (c) $E_{a-G}$ (surface growth) and (d) $E_{a-L}$ (ligand-nanoparticle binding) as a function of dimeter (corresponding to Figure 9 in the main manuscript). The rate constants shown in Figure S24 are time-independent. Note that the $\Delta H_L$ and $\Delta H_G$ remain constant once the nanoparticle size gets larger than 2 nm and this has been considered in our model. The values of $\alpha_L$ and $\alpha_G$ are 0.3 similar to the case of coverage-dependent growth rate constant.

**Model Predictions for the Case of Size-Dependent Growth Rate Constant for Pd Nanoparticles Synthesis in Pyridine**

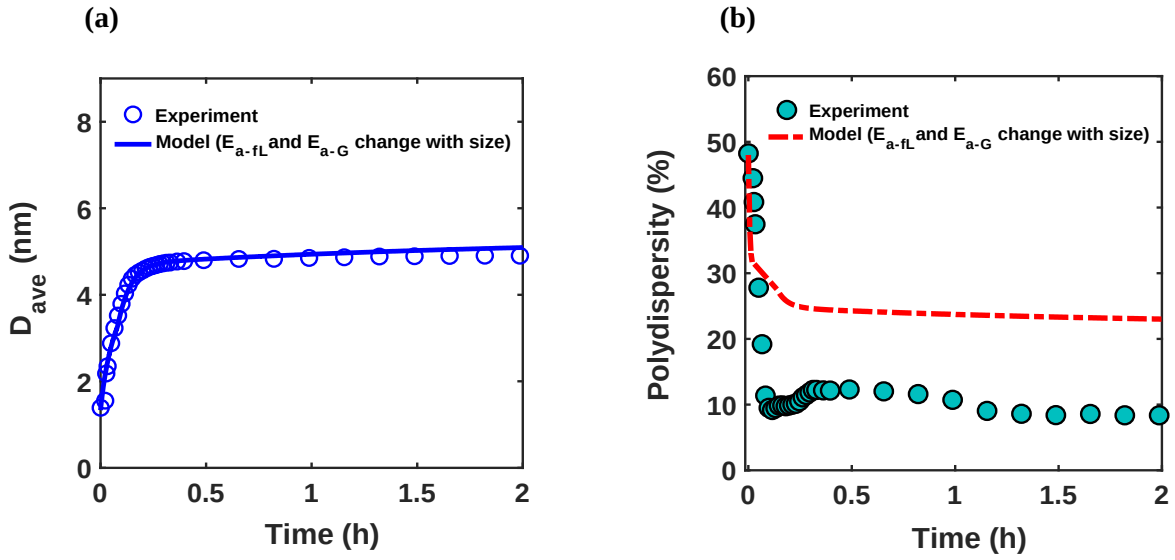


**Figure S25. Model predictions for the case of size-dependent growth rate constant for Pd nanoparticles synthesis in pyridine.** Time evolution of (a) average diameter; (b) polydispersity ($P(t) = \frac{\sigma(t)}{D_{ave}(t)}$) for the case of size-dependent adsorption energies. The size affects both the enthalpy and activation energies for ligand-nanoparticle binding and surface growth. For the 2 nm nanoparticles, we used $\Delta H_{0-L}$=−260 kJ/mol (which is similar to the value obtained from Pd(111) DFT calculations shown in Figure 7) and $E_{a-L0}$ =25 kJ/mol; and then we estimated the $\Delta H_L$ and $E_{a-L}$ value for the smaller nanoparticles (i.e. more exothermic). Regarding the growth enthalpy, for the 0.6 nm nanoparticles, we used $\Delta H_{0-G}$=−251 kJ/mol (as shown in Figure S23) and $E_{a-G0}$=25 kJ/mol; and then we estimated the $\Delta H_G$ and $E_{a-G}$ values for the larger nanoparticles using the trend shown in Figure S23. The values of $\alpha_L$ and $\alpha_G$ are 0.3 similar to the case of coverage-dependent growth rate constant. Experimental conditions: 10 mM $Pd(OAc)_2$ in 1:1 pyridine:hexanol, TOP:Pd=1, and T= 100 °C.

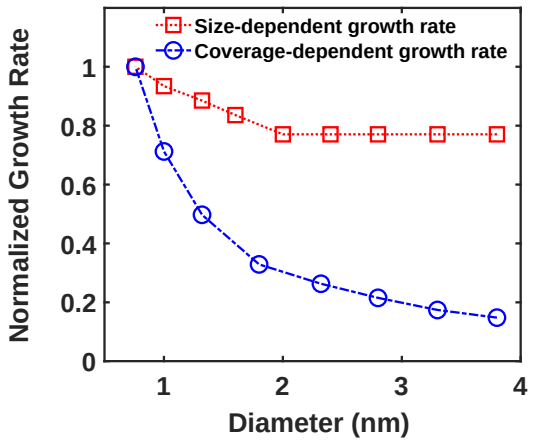


**Figure S26. Model prediction of normalized growth rate for the cases of size- and coverage-dependent growth rate constant.** (i) size-dependent growth rate constant, and (ii) coverage-dependent growth rate constant as a function of diameter at time=0.10 h. The growth rate of different size nanoparticles is normalized to the corresponding growth rate of 0.8 nm nanoparticles in each case.

## References


1. C. A. Dreiss, K. S. Jack and A. P. Parker, *Journal of applied crystallography*, 2006, **39**, 32-38.
2. M. Wuithschick, A. Birnbaum, S. Witte, M. Sztucki, U. Vainio, N. Pinna, K. Rademann, F. Emmerling, R. Kraehnert and J. Polte, *ACS Nano*, 2015, **9**, 7052-7071.
3. M. Kotlarchyk, R. B. Stephens and J. S. Huang, *The Journal of Physical Chemistry*, 1988, **92**, 1533-1538.
4. T. Li, A. J. Senesi and B. Lee, *Chemical Reviews*, 2016, **116**, 11128-11180.
5. X. Chen, J. Schröder, S. Hauschild, S. Rosenfeldt, M. Dulle and S. Förster, *Langmuir*, 2015, **31**, 11678-11691.
6. K. Adachi and H. Watarai, *Journal of Materials Chemistry*, 2005, **15**, 4701-4710.
7. S. Mozaffari, W. Li, C. Thompson, S. Ivanov, S. Seifert, B. Lee, L. Kovarik and A. M. Karim, *Nanoscale*, 2017, **9**, 13772-13785.
8. S. Mozaffari, W. Li, C. Thompson, S. Ivanov, S. Seifert, B. Lee, L. Kovarik and A. M. Karim, *Journal of visualized experiments: JoVE*, 2018.
9. G. Ertl, H. Knözinger and J. Weitkamp, 1997.
10. M. Harada, N. Tamura and M. Takenaka, *The Journal of Physical Chemistry C*, 2011, **115**, 14081-14092.
11. L. Wu, H. Lian, J. J. Willis, E. D. Goodman, I. S. McKay, J. Qin, C. J. Tassone and M. Cargnello, *Chemistry of Materials*, 2018, **30**, 1127-1135.
12. B. Abécassis, F. Testard, O. Spalla and P. Barboux, *Nano Letters*, 2007, **7**, 1723-1727.
13. I. Breßler, B. R. Pauw and A. F. Thünemann, *Journal of applied crystallography*, 2015, **48**, 962-969.
14. Y. Jiang, Y. Huang, H. Cheng, Q. Liu, Z. Xie, T. Yao, Z. Jiang, Y. Huang, Q. Bian, G. Pan, Z. Sun and S. Wei, *The Journal of Physical Chemistry C*, 2014, **118**, 714-719.
15. B.-H. Wu, H.-Y. Yang, H.-Q. Huang, G.-X. Chen and N.-F. Zheng, *Chinese Chemical Letters*, 2013, **24**, 457-462.
16. D. Tomanek, S. Mukherjee and K. Bennemann, *Physical Review B*, 1983, **28**, 665.
17. Z. Yan, M. G. Taylor, A. Mascareno and G. Mpourmpakis, *Nano letters*, 2018, **18**, 2696-2704.